# Topological effects on dynamics in complex pulse-coupled networks of integrate-and-fire type

Maxim S. Shkarayev,[1] Gregor Kovačič,[1] and David Cai[2,3,*]

[1]*Mathematical Sciences Department, Rensselaer Polytechnic Institute, 110 8th Street, Troy, New York 12180, USA*

[2]*Department of Mathematics and Institute of Natural Sciences, Shanghai Jiao Tong University, Dong Chuan Road 800, Shanghai 200240, China*

[3]*Courant Institute of Mathematical Sciences and Center for Neural Science, New York University, 251 Mercer Street, New York, New York 10012, USA*

(Received 15 May 2011; revised manuscript received 31 January 2012; published 12 March 2012)

For a class of integrate-and-fire, pulse-coupled networks with complex topology, we study the dependence of the pulse rate on the underlying architectural connectivity statistics. We derive the distribution of the pulse rate from this dependence and determine when the underlying scale-free architectural connectivity gives rise to a scale-free pulse-rate distribution. We identify the scaling of the pairwise coupling between the dynamical units in this network class that keeps their pulse rates bounded in the infinite-network limit. In the process, we determine the connectivity statistics for a specific scale-free network grown by preferential attachment.

DOI: 10.1103/PhysRevE.85.036104 PACS number(s): 89.75.Fb, 87.19.lj, 05.20.Dd, 87.19.lp

## I. INTRODUCTION

Pulse-coupled network models have found applications in fields ranging from engineering to biology [1–9]. The topology of the couplings between the interacting dynamical units of such networks is typically highly complex and can only be captured statistically. These networks are described as directed graphs, with the dynamical units as the nodes or vertices and their couplings as the edges. The basic statistical quantities of the graph topology, which is also known as the network's *architectural connectivity*, are given in terms of the distributions of the *node degrees* and *edge types*. Each node in a directed graph has an *incoming* and an *outgoing degree*, which are the numbers of directed edges that terminate at and originate from this node, respectively. The total degree of a node is the sum of its incoming and outgoing degrees. The edge type of a specific edge refers to the degrees (incoming, outgoing, or total, depending on the desired description) of the nodes it connects.

In many networks of scientific or practical importance, the node-degree distributions are believed to satisfy simple asymptotic laws, such as power laws. For example, if the exponent $\gamma$ in a negative power law stays in the interval $2 < \gamma \leqslant 3$, the network satisfying this distribution is called *scale-free* [10–13]. Scale-free network architecture is particularly appealing in that it describes networks with many low-degree nodes but also a few large-degree *hubs*, each of which is connected to a substantial portion of the network.

Pulse-coupled models of *integrate-and-fire* (IF) type [5,6] have been used successfully as dynamical units designed to capture a number of robust *network* effects in large-scale neuronal assemblies, for example in the primary visual cortex [14–19]. While the bulk geometric features of the architectural connectivity in such assemblies are quite well known experimentally [20–28], the statistics of the neuronal connectivity degrees are typically unknown and are largely guessed from an indicator of *functional connectivity* [29–36]. Such an indicator is any measurable quantity, for example, the firing rate or subthreshold membrane-potential correlations in neuronal networks, which is believed to depend on the underlying node-connectivity degrees in a monotonically increasing manner. The relationship between networks' architectural and functional connectivities is not yet well understood and deserves a closer look. Therefore, it is important to understand how an indicator of functional connectivity, such as the pulse rates of its dynamical units, depends on the architectural connectivity of a given complex IF network.

The description of large pulse-coupled networks frequently simplifies in the infinite-network limit. However, crucial dynamical properties of such networks, for example, their units' pulse rates, may only remain within a physically relevant regime and therefore yield a meaningful theoretical description in this limit if the strengths of the couplings among the dynamical units in the network obey an appropriate scaling law, which decays with increasing network size. For all-to-all coupled IF networks, this scaling law is inversely proportional to the network size [37,38]. For IF networks with complex topologies, the question of its precise form should be systematically addressed.

In this paper, we address both the question of the dependence of an IF network's pulse rate on its architectural connectivity and the scaling of the network coupling that yields a meaningful description of this dependence in the large-network limit. We use the conductance-based IF model [5,6] to describe the pulse-coupled dynamics of the dynamical units located at the network nodes. Comparing with numerical simulations of this model, we find that an *explicitly solvable* coarse-grained, mean-field limiting description [37–40] of the model network renders asymptotic scaling laws connecting the external input, node degree, and the pulse rates of the dynamical units with high incoming degrees. Instrumental in this analysis is the observation that these units operate in the regime in which they receive strong combined driving from the external input and other units in the network. We also, in this paper, derive a generalization of the mean-field IF network description of [37–40] to the case of networks with complex connectivity topology, which we use in our investigation.

Throughout this paper, we use several terms from neuroscience, because these terms are standard and well suited for

*cai@cims.nyu.edu

 

pulse-coupled networks of IF type and also because our study was motivated by complex neuronal networks. In particular, for simplicity, we call the directed couplings between dynamical units synapses or synaptic connections, with the presynaptic node originating and the postsynaptic node receiving pulses along their connection.

The main results of this paper address the question of how the pulse rate of the dynamical units depends on the underlying connectivity statistics in three example complex IF networks of increasingly complex topology, which include an uncorrelated network [11] and two scale-free networks grown through preferential attachment [41–43]. While these networks are sufficiently idealized to allow for explicit solution, they also progressively incorporate features conjectured to be present in realistic neuronal networks, including scale-free distribution of incoming node degrees and clustering [32–34,36,44–47]. We contrast the dependence of the units' pulse rate on the underlying connectivity statistics in these three networks with the corresponding dependence in the all-to-all connected IF network. In the process, we also derive the edge-type distribution function for the scale-free network of [41].

For the nodes with high incoming degree in both the uncorrelated network [11] and the network of [41], we find that their pulse rates depend linearly on their incoming degree. We also find that the slope of this dependence is controlled by the average incoming degree of the nodes presynaptic to the nodes with a given incoming degree in the uncorrelated network, and the effective version of this average degree in the scale-free network of [41]. This effective degree is induced dynamically by the topological correlations in the network. In both cases, this degree also governs the scaling of the coupling coefficient that preserves finite pulse rates in the large-network limit. Moreover, for the network of [41], we observe that the mean-field model describes averages over ensembles of such networks rather than individual network realizations, and discuss how this model can be modified to apply to each individual realization. For the asymmetric, treelike, unidirectionally scale-free network of [42,43], we find a superlinear power-law dependence of the pulse rate on the incoming node degree, and the absence of any need for scaling the coupling coefficient in the large-network limit. Finally, for both scale-free networks, we derive that their pulse rates are also distributed according to a power law.

In general, for pulse-coupled networks of IF type, we derive that the growth of the pulse rates as a function of the growing node degree can only be linear or superlinear in the asymptotic limit of large node degrees. We then identify a large class of IF networks with properties plausibly mimicking realistic neuronal networks, which we term *boundedly correlated* and *statistically symmetric* (terms defined in Sec. V) and for which we can derive an upper bound on the network coupling strength that guarantees bounded pulse rates of all the dynamical units and another upper bound that is necessary for the pulse rate averaged over the network to remain bounded in the large-network limit. Using the uncorrelated network [11] and the scale-free network of [41], we find that these bounds are the sharpest possible. As mentioned above, we use the asymmetric, unidirectionally scale-free network that we had studied in Ref. [43] to demonstrate superlinear asymptotic pulse-rate dependence on the underlying node degrees, and to illustrate that the coupling-strength scaling does not have to decrease toward zero as the network size approaches infinity in a network that is not statistically symmetric.

The remainder of the paper is organized as follows. In Sec. II, we introduce the two main statistical quantities we use in the network connectivity description. In Sec. III, we describe IF networks with complex topology, the mean-field model used to describe their pulse rate, the linearization of this model for large input values, and the formal solution of the resulting linear model by a Liouville-Neumann series. In Sec. IV, we apply this general theory to three specific networks—all-to-all coupled in Sec. IV A, uncorrelated in Sec. IV B, and scale-free in Sec. IV C—and also find the scalings for their coupling coefficients that keep the pulse rates of their nodes bounded. We describe an additional scale-free network whose properties contrast those of the first three networks in Sec. IV D. In Sec. V, we derive a linear lower bound on the pulse rate as a function of the node degree and generalize the coupling-coefficient scalings found in the previous section to two broad classes of networks. In Sec. VI, we briefly discuss the pulse-rate distributions in our example networks. In Sec. VII, we conclude the paper with a discussion of the results. Technical derivations are relegated to the appendixes. In particular, in Appendix A, we derive the mean-field model for computing the network pulse rate. In Appendix B, we derive the edge-type distribution function for the scale-free network describe in Sec. IV C. In Appendix C, we derive the leading-order pulse-rate behavior for the scale-free network of Sec. IV D. Finally, in Appendix D, we derive the scaling bounds for the network coupling needed to ensure that the individual nodes' and network pulse rate remain bounded, as presented in Sec. V.

## II. NETWORK DESCRIPTION

To investigate the pulse rates of the nodes in the network, we must use information about their incoming degrees. This is because the total network pulse train received by a node is the sum of the pulse trains originating at all its presynaptic nodes, and that is one of the most important factors in determining the node's pulse rate. The most fundamental quantity describing the network statistics that is used in determining the nodes' pulse rates is therefore the distribution of the network nodes' incoming degree, $k$, denoted by $P_{\text{in}}(k)$. In what follows, we frequently refer to $P_{\text{in}}(k)$ simply as the node-degree distribution, and to nodes with incoming degree $k$ as $k$ nodes. In addition to the node-degree distribution, in order to compute the nodes' pulse rates, we also need to know the distribution of the types of edges present in the network. This distribution is usually given by the function that describes the probability, $T(n,k)$, of finding an edge that originates at an $n$ node and terminates at a $k$ node [48]. The distribution $T(n,k)$ is also known as the degree-correlation function [11].

For a network of size $N+1$, evaluating the probability of an edge terminating at a $k$ node allows us to relate the node-degree and edge-type distributions, $P_{\text{in}}(k)$ and $T(n,k)$, respectively, by the equation

$$\int_0^N T(n,k)dn = \frac{kP_{\text{in}}(k)}{\mu}, \tag{1}$$

where

$$\mu \equiv \int_0^N k P_{\rm in}(k) dk \tag{2}$$

is the mean node degree in the network. In particular, Eq. (1) states that the probability of finding an edge that terminates at a $k$ node is proportional to the probability of a $k$ node existing in the network, times $k$, the number of edges that terminate at a $k$ node. Moreover, this interpretation of the right-hand side of Eq. (1) and an application of the Bayes formula imply that the conditional probability, $P(n \mid k)$, of an edge to originate at an $n$ node given that it terminates at a $k$ node equals

$$P(n \mid k) = \frac{\mu T(n,k)}{k P_{\rm in}(k)}, \tag{3}$$

provided that $k \neq 0$. Clearly, $P(n \mid 0) = 0$, since a 0 node receives no synaptic input from other nodes in the network. In what follows, we therefore consistently interpret the right-hand side of formula (3) as vanishing for $k = 0$.

## III. PULSE RATE OF $k$ NODES

In a network of $N+1$ coupled nodes, described by the conductance-based, all-excitatory IF point-neuron model [5,6], the activity $v^i(t)$ of the $i$th node is governed by the equation

$$\tau \frac{dv^i}{dt} = -(v^i - V_r) - G^i(t)(v^i - V_E), \tag{4}$$

until it reaches the threshold value, $V_T$, when it is instantaneously reset to the reset value, $V_r$. At that moment, the $i$th node sends a pulse to every other node in the network, as described below. The remaining parameters in Eq. (4) include $V_E$, the reversal activity value, $\tau$, the activity time constant, and $G^i(t)$, the pulse train

$$G^i(t) \equiv f \sum_j G(t - t_{ij}) + S \sum_{\kappa_i} \sum_j G\left(t - t_j^{\kappa_i}\right), \tag{5}$$

in which the sums extend over all the pulses that the $i$th node receives. Here the pulse shape $G(t)$ is given by an $\alpha$-type function, described further below and in Appendix A.

The first sum in the pulse train $G^i(t)$ in Eq. (5) corresponds to pulses generated by the external drive at times $t_{ij}$, which we assume to form a Poisson train with rate $\nu$. We assume the Poisson pulse trains generated by the external drive arriving at different nodes to be statistically independent. The second sum in the pulse train $G^i(t)$ in Eq. (5) corresponds to pulses arriving at the $i$th node from its presynaptic network nodes along the directed edges determined by the specific network topology. The time $t_j^{\kappa_i}$ corresponds to the $j$th time the $\kappa_i$th presynaptic node of the $i$th node emitted a pulse. Since the nodes in a complex network differ from each other in the number of incoming connections, $k$, if the $i$th node is a $k$ node, the index $\kappa_i$ in the second sum of Eq. (4) will run over its $k$ presynaptic nodes. The coupling strengths are set to $f$ for the pulses arriving through the external drive and $S$ for those arriving from the network nodes.

In our numerical simulations, we solve Eq. (4) using the modified second-order Runge-Kutta algorithm of [49]. For the pulse shape $G(t)$, we use the function

$$G(t) = \Theta(t) \frac{t}{\tau_g^2} e^{-t/\tau_g}, \tag{6}$$

where $\Theta(\cdot)$ is the Heaviside function and $\tau_g$ is the pulse decay rate. For the network parameters, we use the following dimensionless values:

$$V_r = 0, \quad V_T = 1, \quad V_E = 14/3, \tag{7a}$$

$$\tau = 0.02, \quad \tau_g = 0.003. \tag{7b}$$

The activity constants are taken to be shifted and nondimensionalized versions of the typical neuronal reset, threshold, and excitatory reversal potentials of $-70$, $-55$, and 0 mV, respectively, rounded to a close rational number. The time scales are taken to be the typical neuronal leakage-conductance time scale of 20 ms and the AMPA[2-amino-3-(5-methyl-3-oxo-1,2-oxazol-4-yl)propanoic acid]-conductance decay rate of 3 ms.

For a time-independent Poisson rate, $\nu$, of the external drive, when the input fluctuations induced by both the external-drive and the network pulses are small, one can describe the network dynamics by the nodes' pulse rates alone using a mean-field model. In a complex network, the average pulse rate per node, $m_k$, of the $k$ nodes has to be considered separately for every incoming degree $k$. A kinetic-theoretic derivation, described in Appendix A, yields for the pulse rate $m_k$ the mean-field equation

$$\tau m_k = \frac{1 + g_k}{\ln\left(\frac{g_k(V_E - V_r)}{g_k(V_E - V_T) - V_T + V_r}\right)}, \tag{8a}$$

with

$$g_k \equiv f\nu + Sk\mu_k \tag{8b}$$

and

$$\mu_k \equiv \int_0^N P(n \mid k) m_n dn. \tag{8c}$$

Here $g_k$ is the average input to a $k$ node, $\mu_k$ is the average input that a $k$ node is expected to receive from any other type of a node, and $P(n \mid k)$ is the conditional probability of an edge to originate at an $n$ node given that it terminates at a $k$ node, described in Eq. (3). Note that here we approximate $n$ and $k$ as continuous variables.

We are interested in the influence of the network topology statistics on the distribution of the pulse rates $m_k$ corresponding to the nodes with different connectivity degrees, $k$. The properties of this distribution can be brought out most simply in the high-$g_k$ limit, that is, when the average inputs $g_k$ to the nodes are strong, $g_k \gg 1$. We can then Taylor expand the right-hand side of Eq. (8a) in $1/g_k$, and keep only the $O(1)$ terms, to obtain the following linear asymptotic approximation of the original system (8a):

$$m_k \tau \ln A = 1 + \frac{1 - A}{\ln A} + g_k, \tag{9}$$

where

$$A \equiv \frac{V_E - V_r}{V_E - V_T}. \tag{10}$$

Note that in the numerical simulations, we use

$$A = \tfrac{14}{11} = 1.2727, \tag{11}$$

and the parameter values in Eqs. (7a) and (7b).

For a feedforward node, that is, one whose input consists only of its external drive, we have $g_k = f\nu$, and so its pulse rate equals

$$\psi \equiv \frac{1 + (1 - A)/\ln A + f\nu}{\tau \ln A}. \tag{12a}$$

Using this feedforward-node pulse rate and the rescaled coupling constant

$$\lambda \equiv \frac{S}{\tau \ln A}, \tag{12b}$$

we rewrite Eq. (9) as

$$m_k = \psi + \lambda \int_0^N K(k,n) m_n dn, \tag{13}$$

where the kernel,

$$K(k,n) \equiv k P(n \mid k) = \mu \frac{T(n,k)}{P_{\text{in}}(k)}, \tag{14}$$

gives the average number of edges that a $k$ node receives from $n$ nodes, that is, the average number of $n$ nodes presynaptic to a $k$ node.

Equation (13) is a Fredholm integral equation of the second kind. Formally, its solution can be obtained using the Liouville-Neumann series [50]

$$m_k = \sum_{i=0}^{\infty} \lambda^i \phi_i(k), \tag{15}$$

in which $\phi_0 = \psi$ and all the subsequent terms are given by the recursively defined integrals

$$\phi_i(k) \equiv \int_0^N K_i(k,n) \psi dn, \tag{16a}$$

with the first iterated kernel defined as

$$K_1(k,n) = K(k,n) \tag{16b}$$

and the rest as

$$K_i(k,n) \equiv \int_0^N \int_0^N \cdots \int_0^N K(k,y_1) \times K(y_1,y_2) \ldots K(y_{i-1},n) dy_1 \ldots dy_{i-1}. \tag{16c}$$

Trivially, $\phi_1(k) = \psi k$.

Note that, analogously to the kernel $K(k,n)$, the $i$th iterated kernel $K_i(k,n)$ represents the average number of $n$ nodes from which pulses reach a $k$ node via precisely $i$ synaptic connections. Thus, the terms of the series in Eq. (15) possess a clear physi(ologi)cal meaning: The $i$th term represents the contribution to the pulse rate $m_k$ of the external drive transmitted through precisely $i$ synaptic connections. In particular, as expected, $\psi$ is the portion of the pulse rate due to the external drive alone, and thus also the pulse rate of the 0 nodes, that is, those that do not receive any input from other nodes. Therefore, $m_0 = \psi$.

In what follows, we use the series (15) to analyze the linear asymptotes of the pulse rates $m_k$ in three different networks, of which the third has a nontrivial topology. Therefore, this last network also has nontrivial distributions $P_{\text{in}}(k)$ of node degrees and $T(n,k)$ of edge types, the latter of which we evaluate in Appendix B. In addition, we see how the convergence properties of the series (15) imply important bounds on the scaling of the network coupling constant, $S$, in order for the nodes' pulse rates to remain bounded in the large-network limit.

Finally, we mention that one way of quantifying the network activity is the gain function of the entire network, that is, the functional dependence of the mean pulse rate across the network,

$$\bar{m} \equiv \int_0^N m_k P_{\text{in}}(k) dk, \tag{17}$$

on the external input strength $f\nu$. We investigate the properties of this quantity for the networks studied below as well.

## IV. SPECIFIC NETWORKS

In this section, we apply the general approach developed in the previous section to analyzing the dependence of the pulse rates $m_k$ on the node and edge statistics in four different networks of increasing complexity. In the next section, we then generalize the properties of the first three networks to obtain bounds on the scaling of the network coupling, $\lambda$ or $S$, such that the individual pulse rates, $m_k$, and the average pulse rate in the network, $\bar{m}$, remain bounded in the large-network limit, $N \gg 1$.

### A. All-to-all coupled network

For an all-to-all coupled network of IF nodes, $N + 1$ in total, with each pair of nodes connected by a pair of directed edges, the system in Eqs. (8) simplifies considerably. In particular, all the nodes in the network have the same degree, $k = N$, which is thus the only degree we need to consider in Eqs. (8). As a consequence, the only nonzero pulse rate and average input are $m_N$ and $g_N$, respectively. We also have $P(n \mid N) = \delta(n - N)$ (and $P(n \mid k) = 0$ for all other degrees $k$), signifying the fact that the only possible presynaptic nodes are $N$ nodes. Therefore, Eqs. (8) simplify to [38]

$$\tau m_N = \frac{1 + g_N}{\ln\left(\frac{g_N(V_E - V_r)}{g_N(V_E - V_T) - V_T + V_r}\right)}, \tag{18a}$$

with

$$g_N = f\nu + SNm_N. \tag{18b}$$

While the system (18) cannot be solved explicitly for the average pulse rate $m_N$ of the nodes in terms of the external driving strength $f\nu$, the gain curve depicting the relationship of these two quantities can be parametrized exactly by using the input $g_N$ as a parameter [51]. The pulse rate $m_N$ is parametrized via Eq. (18a), and the driving strength $f\nu$ using the parametrization of $m_N$ and Eq. (18b), with $g_N > A - 1$. The resulting gain curves for different values of the coupling strength $S$ are shown in Fig. 1. They rise from the point

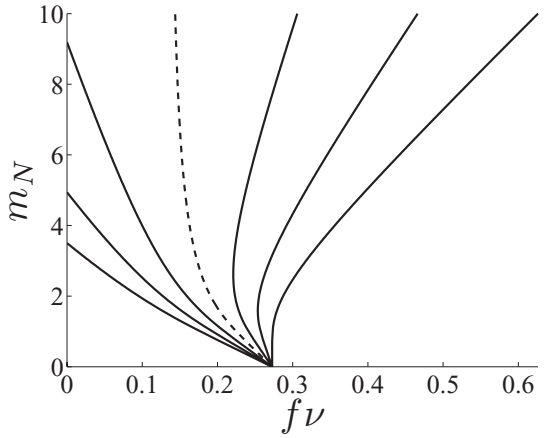


FIG. 1. Gain curves depicting the pulse rate $m_N$ as a function of the driving strength $f\nu$ in the mean-driven limit of the all-to-all coupled network. The parameter values are (7) and (11). The coupling strengths $SN$ along the gain curves are (left to right) 0.096, 0.08, 0.064, $\tau \ln A = 0.048\,23$, 0.032, 0.016, and 0. The gain curves approach straight-line asymptotes; their equations are given by Eq. (19). The asymptote of the gain curve corresponding to the coupling strength $SN = \tau \ln A$ is vertical. Numerical simulations in Ref. [51] indicate that backward-sloping segments of the gain curves are unstable.

$(f\nu, m_N) = (A - 1, 0)$, at least at first slope backward, and eventually tend toward the straight-line asymptotes

$$m_N = \frac{f\nu + 1 - (A-1)/\ln A}{\tau \ln A - SN}. \tag{19}$$

Note that the backward-sloping segments of the gain curves are unstable and are not observed in simulations. Instead, when a gain curve has both backward- and forward-sloping segments, simulations exhibit hysteretic, bistable behavior [37,38,51]. The coupling value

$$S = \frac{\tau \ln A}{N} \tag{20}$$

corresponds to a critical case with a vertical asymptote in the gain curve. For larger values of $S$ there is no nontrivial stable equilibrium solution of Eqs. (18).

The kernel $K(k,n)$ in Eq. (14) for the all-to-all coupled network is only nonzero for $k = N$, in which case it equals $K(N,n) = N\delta(n - N)$, again signifying the fact that all presynaptic nodes are $N$ nodes. The asymptotic integral equation (13) in this case becomes

$$m_N = \psi + \lambda N m_N, \tag{21}$$

with the parameters $\psi$ and $\lambda$ as in Eqs. (12a) and (12b), respectively, and the solution

$$m_N = \frac{\psi}{1 - \lambda N}, \tag{22}$$

which is easily seen to be the same as the straight-line asymptote (19). This solution becomes singular when $\lambda = 1/N$, which is the same as Eq. (20) and is consistent with the commonly used scaling in the mean-field analysis of all-to-all coupled networks. The factor $N$ in the denominator of Eq. (22) can be interpreted in several different ways; the most fruitful is as the number of presynaptic nodes to any given node, as can be seen from the discussion following Eq. (15).

The above discussion of the linearized equation (21) again shows that in the limit of large network size, $N \gg 1$, the network coupling coefficient, $S$, must scale as $O(1/N)$ so that a nontrivial interval of $S$ values will exist in which the network has a stable, nonzero steady state for sufficiently large values of the external driving strength, $f\nu$. As shown in Ref. [51], the network is stable in this state in the sense that the pulse rate remains steady and does not grow in time without a bound.

### B. Uncorrelated network

In this section, we use the Liouville-Neumann series (15) to obtain the exact solution of Eq. (13) for uncorrelated networks [11,52–55], that is, those in which

$$T(n,k) = \frac{k P_{\text{in}}(k) n P_{\text{in}}(n)}{\mu^2}. \tag{23}$$

For uncorrelated networks, Eq. (3) immediately implies that the conditional probability $P(n \mid k)$ for an edge to originate from an $n$ node given that it terminates at a $k$ node equals $P(n \mid k) = n P_{\text{in}}(n)/\mu$ and thus is independent of the degree $k$. This, in turn, implies that the kernel in Eq. (14) equals $K(k,n) = kn P_{\text{in}}(n)/\mu$, that is, $k$ times the probability of an edge terminating at an $n$ node. Therefore, for the $i$th coefficient $\phi_i(k)$ in the Liouville-Neumann series (15), we find from Eqs. (16) the expression

$$\phi_i(k) = k\psi \left( \frac{\langle n^2 \rangle_N}{\mu} \right)^{i-1}, \tag{24}$$

where

$$\langle n^2 \rangle_N = \int_0^N n^2 P_{\text{in}}(n) dn \tag{25}$$

is the second moment of the incoming-degree distribution, $P_{\text{in}}(n)$. From Eqs. (3) and (23), we note that, in an uncorrelated network, the ratio $\langle n^2 \rangle_N/\mu$ in Eq. (24) equals the average incoming degree of the nodes presynaptic to a $k$ node,

$$\int_0^N n P(n \mid k) dn = \frac{\langle n^2 \rangle_N}{\mu}. \tag{26}$$

Clearly, this expression is independent of the postsynaptic node's incoming degree $k$ and thus is the same for all nodes in the uncorrelated network. (The exceptions, of course, are the 0 nodes, which have no presynaptic nodes.)

From Eq. (24), it follows that the average pulse rate $m_k$ of a $k$ node satisfies the asymptotic relation

$$m_k = \psi \left( 1 + \frac{\lambda k}{1 - \lambda \langle n^2 \rangle_N/\mu} \right). \tag{27}$$

From Eq. (12a), we immediately note that the asymptotic pulse rate $m_k$ in Eq. (27) depends on both the driving strength $f\nu$ and the incoming node degree $k$ in a linear fashion. In particular, the slope of the linear asymptote approached by the $m$-versus-$f\nu$ gain curve for the average pulse rate $m_k$ of a $k$ node is proportional to its degree $k$, with the $k$-independent proportionality constant equaling $\lambda/[\tau \ln A\,(1 - \lambda \langle n^2 \rangle_N/\mu)]$. All these slopes become infinite at the same value of the coupling parameter $\lambda$, namely, $\lambda = \mu/\langle n^2 \rangle_N$, the reciprocal

of the average incoming node degree of the nodes presynaptic to any node in the network.

In the large-$N$ limit, we have to rescale the coupling coeffcient $\lambda$ (or, equivalently, $S$) by the reciprocal average presynaptic node degree, $\mu/\langle n^2\rangle_N$, in order for a bounded, nonzero, steady pulse-rate solution to exist for nonvanishing coupling values. Clearly, this scaling also follows directly from the convergence criterion for the Liouville-Neumann series leading to the pulse-rate solution (27).

Averaging the pulse rates $m_k$ in Eq. (27) over the incoming node-degree distribution, $P_{\rm in}(k)$, yields the expression

$$\bar{m} = \psi\left(1 + \frac{\lambda\mu}{1 - \lambda\langle n^2\rangle_N/\mu}\right) \tag{28}$$

for the average pulse rate of the nodes in the network. We see that, under the scaling of the coupling parameter $\lambda$ by the reciprocal average presynaptic node degree $\mu/\langle n^2\rangle_N$, this pulse rate remains bounded for $N \gg 1$ due to the inequality $\langle n^2\rangle_N > \mu^2$.

Finally, the average per-node input rate, $\mu_k$, to a node with incoming degree $k$ can be computed using Eqs. (23), (8c), and (3) as

$$\mu_k = \frac{\psi}{1 - \lambda\langle n^2\rangle_N/\mu}. \tag{29}$$

Since this rate is independent of the node degree $k$, one can see that the average input to a $k$ node, $g_k$ in Eq. (8b), is a linear function of $k$. This implies that, for moderate external drive strength, $f\nu$, the drive of the nodes with low incoming degrees has a substantial *feedforward* component, that is, a substantial direct contribution from the external drive. On the other hand, the drive of the nodes with high incoming degrees is largely *feedback* in that they are predominantly driven by the pulses arriving from their presynaptic nodes.

For scale-free uncorrelated networks [11,55], the second moment $\langle n^2\rangle_N$ of the node-degree distribution $P_{\rm in}(n)$ diverges logarithmically in the large-network limit, $N \gg 1$, while the average node degree $\mu$ remains bounded. In this limit and under the $O(\mu/\langle n^2\rangle_N)$ scaling of the coupling parameter $\lambda$, the pulse rates $m_k$ in Eq. (27) approach the pulse rate $\psi$ of a feedforward node for any fixed node degree $k$ in such a network. The influence of the network pulses is only felt by nodes with degrees $k \gtrsim O(\langle n^2\rangle_N/\mu)$, that is, comparable to or larger than the average presynaptic node degree. Additionally, the $O(\mu/\langle n^2\rangle_N)$ scaling of $\lambda$ implies that the average pulse rate $\bar{m}$ of the nodes in the network approaches that of feedforward nodes for $N \gg 1$. In other words, in a scale-free, uncorrelated network, any node with a fixed incoming degree $k$ only feels the input of the feedforward external drive in the large-network limit, and only nodes with incoming degrees comparable to or larger than the average presynaptic node-degree feel the influence of the network.

### C. Scale-free network

We now calculate the asymptotic pulse rates for a pulse-coupled network with a scale-free architecture. We recall that scale-free networks are defined as those with a power-law asymptotic behavior of the incoming degree distribution, $P_{\rm in}(n) \sim n^{-\gamma}$, where $2 < \gamma \leqslant 3$. In such networks, the mean, $\mu$, of the distribution $P_{\rm in}(n)$ remains finite, while its second moment, $\langle n^2\rangle_N$, diverges as the size of the network increases, that is, for $N \gg 1$.

Since pulse-coupled networks are directed, we must construct this scale-free network in two steps: We first construct the corresponding undirected network following a modified version of the algorithm described in Ref. [41] and then randomly assign a direction to each of its undirected edges. The undirected network of [41] grows in stages: Its first stage is an all-to-all connected network consisting of $\ell$ nodes, which are said to be *active*. At each subsequent stage of the network growth, a new active node is first attached to every active node via an undirected edge, and then an active node is *deactivated* with the probability $\sim 1/n$, where $n$ is its current *total* degree, that is, the number of all undirected edges emanating from it. A direction is assigned randomly to every edge, with probability 1/2.

For the resulting directed network, as we show in Appendix B, if the initial number of active nodes, $\ell$, is large, $\ell \gg 1$, the incoming-degree distribution is well approximated by a scale-free form,

$$P_{\rm in}(k) = \frac{\ell^2}{2k^3}, \tag{30}$$

for the incoming-degree values $\ell/2 \leqslant k \leqslant N/2$ and can be taken to vanish for $k < \ell/2$ and $k > N/2$. Note that, up to terms that decay with $N \gg 1$, for this network

$$\mu = \ell, \quad \langle n^2\rangle_N = \frac{\ell^2}{2}\ln\frac{N}{\ell}, \tag{31}$$

so that its mean node degree is indeed bounded and its second moment diverges logarithmically with increasing network size.

The derivation of the edge-distribution function $T(n,k)$ for this network is also given in Appendix B, where for $\ell \gg 1$ we find that it is well approximated by the expression

$$T(n,k) = \frac{P_{\rm in}(k)P_{\rm in}(n)}{\mu}(n + k - \mu), \tag{32}$$

when $\ell/2 = \mu/2 \leqslant n,k \leqslant N/2$, and can be taken to vanish otherwise.

We again construct the solution for the average pulse rate, $m_k$, of a $k$ node using the Liouville-Neumann series in Eq. (15). First, Eqs. (30), (32), and (3) imply that the conditional probability $P(n\,|\,k)$ for an edge to originate from an $n$ node given that it terminates at a $k$ node equals $P(n\,|\,k) = P_{\rm in}(n)(n + k - \mu)/k$. Therefore, the kernel $K(k,n)$ in Eq. (14) becomes $K(k,n) = P_{\rm in}(n)(n + k - \mu)$. After recalling from Sec. III that the first two coefficients in this series equal $\phi_0(k) = \psi$ and $\phi_1(k) = \psi k$, we show by induction using Eq. (16c) that the $i$th coefficient has the form $\phi_i(k) = \psi[A_i k + B_i]$:

$$\begin{aligned}\phi_{i+1}(k) &= \psi\int_{\ell/2}^{N/2} P_{\rm in}(n)(n + k - \mu)(A_i n + B_i)dn \\ &= \psi[(\mu A_i + B_i)k + \sigma^2 A_i] = \psi\left[A_{i+1}k + B_{i+1}\right],\end{aligned} \tag{33}$$

where $\sigma^2 \equiv \langle n^2\rangle_N - \mu^2$ is the variance of the incoming degree distribution $P_{\rm in}(n)$. Equation (33) immediately implies the recursion relation

$$A_{i+1} = \mu A_i + \sigma^2 A_{i-1}, \tag{34}$$

whose solution, together with the equation $B_{i+1} = \sigma^2 A_i$, yields the coefficients $\phi_i(k)$.

From the form of the coefficients $\phi_0(k) = \psi$ and $\phi_1(k) = \psi k$, we find the initial conditions $A_0 = 0$, $A_1 = 1$, $B_0 = 1$, and $B_1 = 0$. Assuming the solution to the recursion relation in Eq. (34) as $A_i = r^i$, we find that $r$ satisfies the quadratic equation $r^2 - \mu r - \sigma^2 = 0$ and that $A_i$ and $B_i$ satisfying this recursion relation and the initial conditions are given by the expressions

$$A_i = \frac{1}{r_+ - r_-}(r_+^i - r_-^i), \quad i = 0,1,\ldots, \tag{35a}$$

$$B_0 = 1, \quad B_i = \frac{\sigma^2}{r_+ - r_-}(r_+^{i-1} - r_-^{i-1}), \quad i = 1,2,\ldots, \tag{35b}$$

$$r_\pm = (\mu \pm \sqrt{\mu^2 + 4\sigma^2})/2. \tag{35c}$$

Finally, the pulse rate $m_k$ is given by

$$\begin{aligned} m_k &= \sum_{i=0}^{\infty} \lambda^i \psi (A_i k + B_i) \\ &= \frac{\psi}{r_+ - r_-}\left[k\left(\sum_{i=0}^{\infty}\lambda^i r_+^i - \sum \lambda^i r_-^i\right)\right. \\ &\quad \left. +1 + \sigma^2\lambda\left(\sum_{i=0}^{\infty}\lambda^i r_+^i - \sum_{i=0}^{\infty}\lambda^i r_-^i\right)\right] \\ &= \frac{\psi}{r_+ - r_-}\left[(k+\sigma^2\lambda)\left(\frac{1}{1-\lambda r_+} - \frac{1}{1-\lambda r_-}\right) + 1\right] \\ &= \psi\left(1 + \frac{\lambda k + \lambda^2\sigma^2}{1 - \lambda\mu - \lambda^2\sigma^2}\right). \end{aligned} \tag{36}$$

Just as for the uncorrelated network, the asymptotic slopes of the individual gain curves connecting the pulse rate $m_k$ to the external driving strength $f\nu$ are linear in both $f\nu$ and the node degree $k$. All their slopes become infinite simultaneously at the coupling value $\lambda = r_+$. (Note that the Liouville-Neumann series in Eq. (36) ceases to converge at the lower value $\lambda = -r_-$.) Again, in order to retain a nonzero stable steady state in the large-network limit, $N \gg 1$, one must rescale the coupling parameter $\lambda$ in Eq. (12b), and therefore the coupling strength $S$, but now by an $O(1/\langle n^2\rangle_N^{1/2})$ quantity, since $r_+ = O(\langle n^2\rangle_N^{1/2})$.

It is instructive to compare the expression for the pulse rate $m_k$ of this scale-free network, given in Eq. (36), to the corresponding expression for the uncorrelated network, given in Eq. (27). In particular, we see that the incoming node degree $k$ in Eq. (27) is replaced with the *effective* node degree, $k_{\text{eff}} = k + \lambda\sigma^2$, in Eq. (36). Likewise, in the denominator, from Eq. (27), we would expect the coupling constant $\lambda$ to be multiplied by the average incoming degree of a $k$ node's presynaptic nodes,

$$\int_{\ell/2}^{N/2} n P(n\,|\,k) dn = \mu + \frac{\sigma^2}{k} \tag{37}$$

[as computed from Eqs. (30), (32), and (3)]. However, this is not the case. For this correlated network, an *effective* average presynaptic node degree appears as the factor instead, which equals $k_{\text{eff}}^{\text{pre}} = \mu + \lambda\sigma^2$, and is independent of the node degree $k$. Note that, in fact, $k_{\text{eff}}^{\text{pre}}$ equals the average of the effective node degree $k_{\text{eff}}$ over the network, $k_{\text{eff}}^{\text{pre}} = \langle k_{\text{eff}}\rangle_N$. In addition, on account of the scaling of $\lambda$, the effective node degree $k_{\text{eff}}^{\text{pre}}$ is only of size $O(\langle n^2\rangle_N^{1/2})$, which is a much smaller quantity than its $O(\langle n^2\rangle_N/\mu)$ counterpart in Eq. (27) for an uncorrelated network. The effective node and average presynaptic node degrees, $k_{\text{eff}}$ and $k_{\text{eff}}^{\text{pre}}$, depend on the coupling strength, $\lambda$, for this correlated network and are a consequence of the dynamical effects induced by the topological correlations, that is, the fact that the edge-distribution function $T(n,k)$ in Eq. (32) is not of the form (23).

We find the network gain curve by averaging Eq. (36) over $k$:

$$\bar{m} = \frac{\psi}{1 - \lambda\mu - \lambda^2\sigma^2}. \tag{38}$$

Under the above scaling of the coupling parameter $\lambda$, this formula shows that the network-averaged pulse rate of the nodes remains bounded in the large-network limit, $N \gg 1$.

The average per-node input rate to a $k$ node, $\mu_k$, is calculated using Eqs. (36), (8c), and (3) as

$$\mu_k = \frac{\psi}{1 - \lambda\mu - \lambda^2\sigma^2}\left(1 + \frac{\lambda\sigma^2}{k}\right), \tag{39}$$

and the average input to a $k$ node, $g_k$ in Eq. (8b), therefore equals

$$g_k = f\nu + \frac{\psi\lambda\tau \ln A\,(k + \lambda\sigma^2)}{1 - \lambda\mu - \lambda^2\sigma^2}, \tag{40}$$

with the constant $A$ as in Eq. (10). Note that the effective node degree, $k_{\text{eff}}$, also enters $g_k$ as a factor. Therefore, unlike in the uncorrelated network, while $g_k$ is still a linear function of the node degree $k$ in this correlated network, even the input to the nodes with low incoming degrees has a substantial feedback component arising from network interactions. As mentioned above, this feedback component is also reflected in the pulse rates $m_k$ in Eq. (36), as well as the effective degrees $k_{\text{eff}}$ and $k_{\text{eff}}^{\text{pre}}$.

Note that the average input rate that a $k$ node receives from any of its presynaptic nodes, as given in Eq. (39), is a decreasing function of $k$. This may be a consequence of this network's *disassortative* nature [13], that is, the property that the average incoming degree of a $k$ node's presynaptic nodes, given in Eq. (37), decreases with the degree $k$.

To determine how well our theoretical findings, valid in the large-network limit, can describe pulse-coupled dynamics of finite-size networks, we compare them with the results of direct numerical Monte Carlo simulations of Eq. (4). The top panel in Fig. 2 reveals that the mean-pulse-rate formula in Eq. (38) is highly accurate *on average*, that is, not for any given network, but for a large *ensemble* of networks. In particular, $\bar{m}$ in Eq. (38) describes the gain curve expressing the dependence of the average pulse rate of the nodes in such an ensemble on the external driving strength $f\nu$ with great precision.

The bottom panel of Fig. 2 reveals that Eq. (38) also describes the gain curves of the individual network realizations very well, provided the node-degree variance $\sigma^2$, as given in Eq. (31), is replaced by the value of the node-degree variance,

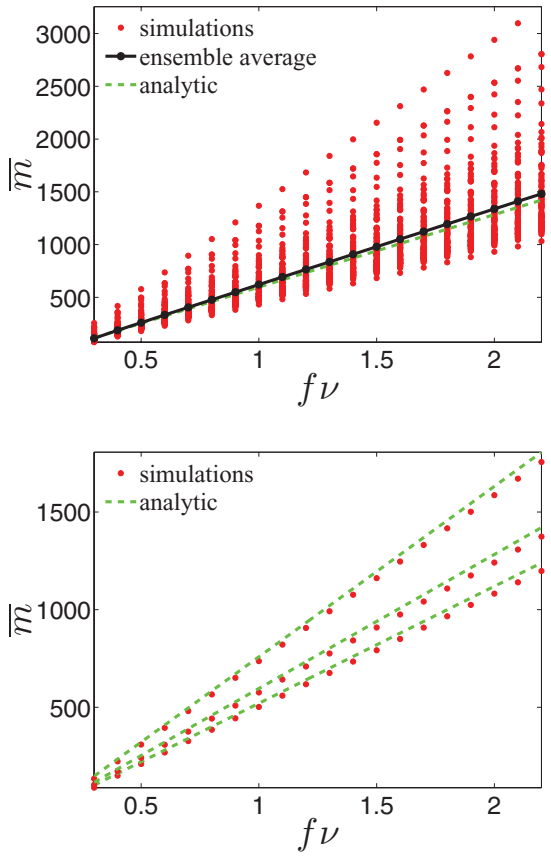


FIG. 2. (Color online) Gain curves for the network discussed in Sec. IV C, size $N = 10^4$, initial size $\ell = 50$. Top: The dots (red online) represent the dependence of the mean network pulse rates, $\bar{m}$, on the external driving strength, $f\nu$, for an ensemble of 100 network realizations. The network size was $10^4$. The solid curve (black online) represents the average $\bar{m}$-versus-$f\nu$ gain curve over the ensemble. The dashed curve (green online) represents the linear gain-curve asymptote predicted by Eq. (38). Bottom: Gain curves depicting the average pulse rate $\bar{m}$ as a function of the external driving strength $f\nu$ for three individual realizations of a network with $10^4$ nodes are represented by dots (red online). The dashed lines (green online) represent the linear gain-curve asymptote predicted by Eq. (38) with the variance $\sigma^2$ in Eq. (31) replaced by the realization variance $\sigma_r^2$ in Eq. (41). The parameter values are those in Eqs. (7) and (11), $S = 4 \cdot 10^{-5}$, $f = 5 \cdot 10^{-5}$.

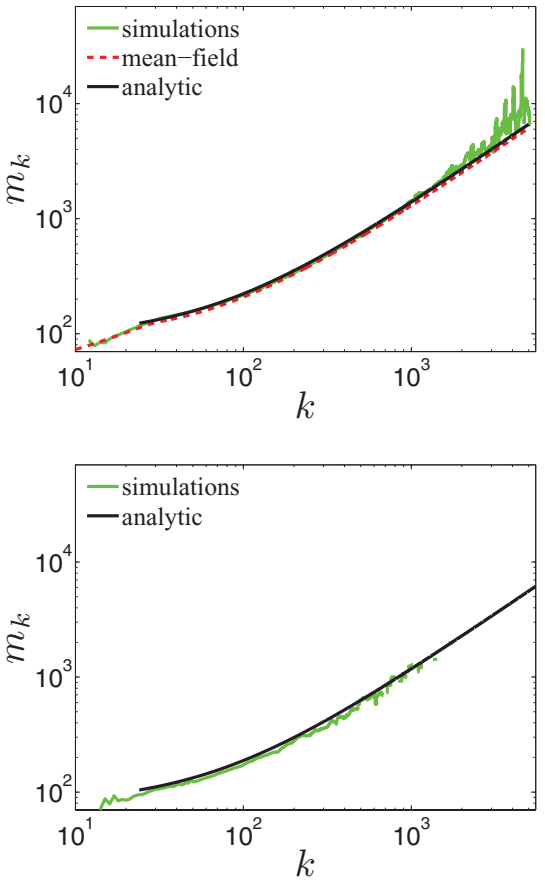


FIG. 3. (Color online) Pulse rate $m_k$ as a function of the incoming node-degree $k$ for the network discussed in Sec. IV C, size $N = 10^4$, initial size $\ell = 50$. Top: Gray solid line (green online) represents $m_k$ averaged over all $k$-nodes in 500 network realizations. Dashed line (red online) represents $m_k$ as computed numerically from Eq. (8a), truncated at $N = 10^4$, with $T(n,k)$ given by Eq. (B31), using the approximation described at the end of Appendix B. Black solid line represents the exact solution (36) of Eq. (9), with $k \geqslant \ell/2$. Bottom: Gray solid line (green online) represents $m_k$ averaged over all $k$-nodes in a single network realization of size $N = 10^4$. Black solid line represents the solution (36) with $k \geqslant \ell/2$ and the variance $\sigma^2$ in Eq. (31) replaced by the realization variance $\sigma_r^2$ in Eq. (41). On both panels, the oscillations exhibited by the simulation results at large values of $k$ are a consequence of the poor statistics due to the scarcity of large-degree nodes in a finite network. The parameter values are those in Eqs. (7) and (11), $S = 4 \cdot 10^{-5}$, $f = 1.8 \cdot 10^{-5}$, $\nu = 2 \cdot 10^4$ ($f\nu = 0.36$).

$\sigma_r^2$, of the particular realization in question. This value is given by the formula

$$\sigma_r^2 = \frac{1}{N}\sum_{j=1}^{N} n_j^2 - \mu^2, \tag{41}$$

where the sum runs over all the nodes in the network and $n_j$ denotes the $j$th node's incoming degree. Since $\sigma^2$ diverges with large network size $N + 1$, the value of its counterpart $\sigma_r^2$ over different network realizations varies greatly, as Fig. 2 shows. The mean node degree, on the other hand, converges to $\mu$ in the large-network limit, and therefore can readily be replaced by $\mu$ in each sufficiently large network realization. It can thus be kept in Eq. (38) when evaluating the gain curve for an individual network realization.

The dependence of the individual pulse rate $m_k$ on the incoming node degree $k$ is described by Eq. (36) in a similar manner. In particular, Eq. (36) provides an accurate description for the average pulse rate of $k$ nodes in a large *ensemble* of networks, as shown in the top panel of Fig. 3. In addition to the comparison of Eq. (36) to direct numerical Monte Carlo simulations of Eq. (4), we also compare it to a finite truncation of the mean-field system (8), with the average input $\mu_k$ in Eq. (8c) evaluated using the more precise formulas (B26) and (B31), as described at the end of Appendix B, rather than using Eqs. (30) and (32). (The truncation size is taken equal to one half of the size of the network realizations.) Equation (36) and this last procedure give results

that are virtually indistinguishable. For an individual network realization, Eq. (36) also provides an accurate description of the relationship between the average pulse rate $m_k$ over all $k$ nodes in the network and the node degree $k$, provided the variance $\sigma^2$, given in Eq. (31), is again replaced by the realization variance $\sigma_r^2$, given in Eq. (41).

### D. Asymmetric scale-free network

The final network that we present has asymmetric incoming- and outgoing-degree distributions. Just as the network in the previous section, this network is again grown in stages, beginning with two nodes and one synaptic connection [42]. At every subsequent stage, one new presynaptic node is connected to one existing network node, which becomes postsynaptic to the new node. The probability that this new node is connected to any given existing node is proportional to this latter node's total connectivity degree. We investigated this network previously in Ref. [43].

As a result of this construction, every node in the network has the outgoing degree 1. On the other hand, as derived in Ref. [42], the nodes' incoming-degree distribution is given by

$$P_{\text{in}}(k) = \frac{4}{(k+1)(k+2)(k+3)}, \tag{42}$$

and their edge-type distribution is given by

$$T(n,k) = \frac{4k}{(n+1)(p+2)(p+3)(p+4)}\left[\frac{1}{n+2} + \frac{3}{p+1}\right], \tag{43}$$

with $p = n + k$. The distribution (42) is asymptotically scale-free for large values of the incoming node degree $k$. Note that the mean node degree equals

$$\mu = 4\sum_{k=0}^{\infty} \frac{k}{(k+1)(k+2)(k+3)} = 1 \tag{44}$$

as a consequence of the network's treelike topology resulting in many nodes with incoming degree 0. [Equation (44) can be shown by decomposing the terms in the sum into partial fractions.] Note also that the second node-degree moment $\langle n^2 \rangle_N$ diverges logarithmically with the network size $N \gg 1$.

For this network, due to the complicated nature of the distribution functions (42) and (43), using the Liouville-Neumann series (15) for analyzing the steady state of the network is impractical. Instead, in the asymptotic limit of high incoming node degree, $k$, and large network size, $N \gg 1$, we find a power-law dependence of the pulse rate $m_k$ on $k$. This dependence is induced dynamically by the underlying asymptotic power-law incoming-degree distribution in the network architecture. In particular, as we describe in Appendix C, inserting into Eq. (13) the ansatz

$$m_k \sim Bk^{\gamma}, \quad \gamma > 1, \quad k \gg 1, \tag{45}$$

an application of residue calculus and a large-$k$ expansion yield the following relation between the exponent $\gamma$ and the network coupling coefficient $\lambda$:

$$\lambda = -\frac{2\sin(\pi\gamma)}{\pi\gamma(\gamma-2)(\gamma-3)}. \tag{46}$$

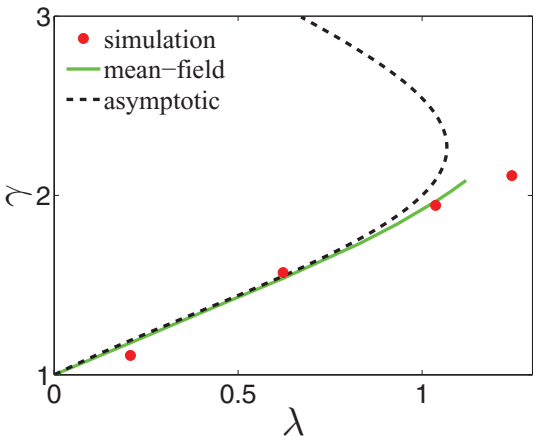


FIG. 4. (Color online) The power $\gamma$ in the asymptotic relationship (45) as computed from Eq. (46) (dashed line, black online), and extracted from the results of the numerical solution of Eq. (8), truncated at $N = 10^4$ (solid line, green online), and direct numerical simulations of one network realization of size $N = 7 \times 10^5$ (dots, red online). The ansatz $m_k = m_0 + Bk^{\gamma}$ was used as a fit. Note that both the solutions of Eq. (8) and the results of the numerical simulations extend beyond $\gamma = 2$ ($\lambda = 1$). The rest of the parameter values are those in Eqs. (7) and (11), $\nu = 2 \times 10^4$, $f = 1.8 \times 10^{-5}$ ($f\nu = 0.36$).

We must require that $\gamma < 4$ so that the pulse rate $m_k$, as computed via Eq. (13), remains finite, and $\gamma > 1$ so that the network coupling is non-negative, $\lambda > 0$. These two requirements single out two possible branches of the dependence of the exponent $\gamma$ on the coupling parameter $\lambda$ in Eq. (46), as shown in Fig. 4. The lower of these two branches is stable, which we have observed in direct numerical simulations of the IF network (4). Note that numerical solutions of the fully nonlinear mean-field model in Eq. (8), as well as the direct numerical simulations of the IF system (4), indicate the existence of these stable gain curves $m_k$ versus $f\nu$ at every point along this branch, which extends above $\gamma = 2$, as can be seen from Fig. 4.

The asymptotic power-law behavior (45) of the pulse rate $m_k$ for large node-degree values $k$ is shown in Fig. 5, which also indicates that this behavior is independent of either the network size in the direct numerical simulations of Eqs. (4) or the numerical truncation size of the mean-field model (8). Numerical solution of the fully nonlinear mean-field model (8) further indicates that the dependence of the leading-order coefficient, $B$, in the power-law solution (45) is asymptotically linear in both the parameters, $\psi$ (i.e., in the external-drive strength $f\nu$) and $\lambda$ (i.e., the network coupling $S$), as depicted in Fig. 6. The linear dependence of $B$ on $\psi$ and $\lambda$ can be deduced form the linear relation exhibited in the each panel of Fig. 6 and also the fact that all the curves in the opposite panel with sufficiently large values of $\psi$ or $\lambda$ overlap with one-another; the curves that do not correspond to values of $\psi$ or $\lambda$ sufficiently small that nonlinear effects take over (cf. the gain curves in Fig. 1).

The independence of the exponent $\gamma$ from the coefficient $\psi$ (i.e., the driving strength $f\nu$), as predicted by Eq. (46), is confirmed in Fig. 7 both using the numerical solution of Eq. (8) and network simulations. In particular, for different values of $f\nu$ but the same value of the network coupling constant $S$,

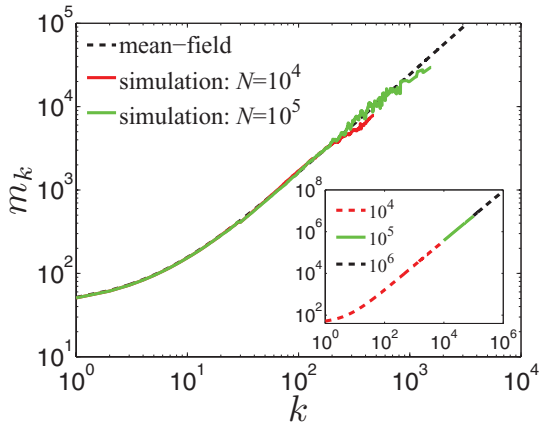


FIG. 5. (Color online) Pulse rate $m_k$ as a function of the incoming node degree $k$ for the network discussed in Sec. IV D. Dark gray solid line (red online) represents the results of direct numerical simulations averaged over 500 realizations of the network of size $N = 10^4$; light gray solid line (green online) represents averages over 50 realizations of the network of size $N = 10^5$. Dashed line (black online) represents $m_k$ as computed numerically from a finite truncation of Eq. (8a), with $T(n,k)$ given by Eq. (43). (Inset) The pulse rate $m_k$ on the incoming node-degree $k$, as computed from a finite truncation of Eq. (8a), does not depend on the truncation size. The truncation sizes used in the computations were $N = 10^4$ (dashes, red online), $N = 10^5$ (solid gray line, green online), $N = 10^6$ (dashes, black online). The parameter values are those in Eqs. (7) and (11), $S = 10^{-3}$, $f = 1.8 \times 10^{-5}$, $\nu = 2 \times 10^4$ ($f\nu = 0.36$).

on the logarithmic scale, the dependence of the pulse rate $m_k$ on the node degree $k$ asymptotes toward parallel straight lines for large $k$, signifying the same $\gamma$. On the other hand, for the same value of $f\nu$ but different values of $S$, the asymptotic slope of the two asymptotes differs, signifying two different

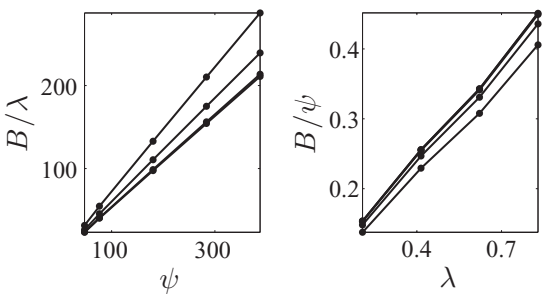


FIG. 6. The dependence of the coefficient $B$ in Eq. (45) on the external drive through the feedforward pulse rate $\psi$ in Eq. (12a) and the network coupling constant $\lambda$ in Eq. (12b), as computed from the mean-field model (8a). The ratios $B/\lambda$ and $B/\psi$ are used to test for linearity. (Left) The values of $\lambda$ along the curves from top to bottom are 0.21, 0.41, 0.62, and 0.83, corresponding to the values of the network coupling $S = 1 \times 10^{-3}$, $2 \times 10^{-3}$, $3 \times 10^{-3}$, and $4 \times 10^{-3}$. The bottom two curves lie on top of each other. (Right) The values of $\psi$ along the curves from top to bottom are 387, 283, 180, 76, and 47, corresponding to the values of the external driving strength $f\nu = 2$, 1.5, 1, 0.5, and 0.36. The top four curves lie on top of each other. The truncation size is $N = 10^4$. The rest of the parameter values are those in Eqs. (7) and (11).

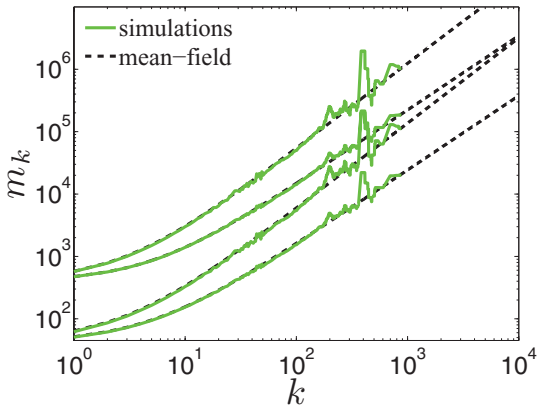


FIG. 7. (Color online) For the same value of the coupling parameter $S$ and two different values of the external drive $f\nu$, the logarithmic dependence of the pulse rate $m_k$ on the node degree $k$ approaches a pair of parallel straight lines for large $k$. This verifies that the exponent $\gamma$ in the asymptotic relationship (45) is independent of $f\nu$. Displayed is the verification for two different values of $S$. Gray solid line (green online) represents the results of direct numerical simulations of one realization of the network of size $N = 7 \times 10^5$. Dashed line (black online) represents numerical solutions of the mean-field equations (8), truncated at $N = 10^4$. From top to bottom, the values of $f\nu$ and $S$ along the curves are $f\nu = 2.0$, $S = 2 \times 10^{-3}$; $f\nu = 2.0$, $S = 10^{-3}$; $f\nu = 0.36$, $S = 2 \times 10^{-3}$; and $f\nu = 0.36$ $S = 10^{-3}$. The rest of the parameter values are those in Eqs. (7) and (11), and $\nu = 2 \times 10^4$.

values of $\gamma$. Figure 7 also confirms the agreement between the numerical solution of Eq. (8) and network simulations.

In addition to being able to find its asymptotic $k$ dependence of its pulse rate $m_k$, we can derive this network's mean pulse rate, $\bar{m}$ in Eq. (17), exactly. In particular, even more generally, let us consider any network in which the outgoing node degree is a constant number $q$, while the incoming degree follows a distribution $P_{\text{in}}(k)$. This is certainly the case for the network at hand, for which $q = 1$. For such a network, the probability $\int_0^N T(n,k)dk$ of finding an edge originating at an $n$ node clearly equals the probability $P_{\text{in}}(n)$ of finding such a node, regardless of the outgoing degree $q$. This observation, together with the definition of the mean network pulse rate in Eqs. (17), (13), and (14) imply the equation

$$\begin{aligned}\bar{m} &= \psi + \lambda\mu \int_0^N m_n dn \int_0^N T(n,k)\, dk \\ &= \psi + \lambda\mu \int_0^N P_{\text{in}}(n) m_n\, dn \\ &= \psi + \lambda\mu\bar{m}. \end{aligned} \tag{47}$$

Therefore, we find

$$\bar{m} = \frac{\psi}{1 - \mu\lambda}. \tag{48}$$

As shown above, for the network at hand, $\mu = 1$, so that the mean pulse rate $\bar{m}$ becomes singular at $\lambda = 1$. Notice, however, that the individual pulse rates $m_k$ are still bounded at $\lambda = 1$, and therefore the origin of the singularity in Eq. (48) is not a singularity in $m_k$. [Recall that the boundedness of $m_k$ follows from Eqs. (45) and (46) and is confirmed by both the

numerical solution of Eq. (8) and numerical simulations of Eqs. (4) with $\gamma > 2$, i.e., $\lambda > 1$, depicted in Fig. 4.] Instead, we see from Eq. (46) that $\gamma \to 2$ as $\lambda \to 1$, which implies that then the integral in $\bar{m} = \int_0^N m_k P(k)\, dk \sim \ln N$ diverges in the limit of large network size. This is in contrast with the networks of Secs. IV B and IV C, whose mean-pulse-rate gain curves become singular precisely when those for the individual pulse rates $m_k$ do.

The discussion in the previous paragraph further shows that no scaling of the coupling constant is needed for this network in the large-size limit in order to maintain stable pulse rates. This is again in contrast with the networks discussed in the preceding sections and is further discussed in the next section.

## V. SCALING BOUNDS FOR NETWORK COUPLING

In this section, we show that the network coupling scalings which we found in Secs. IV B and IV C are not accidental. In fact, for a large class of pulse-coupled networks, they represent the strongest coupling that still guarantees the existence of a stable, nonvanishing, steady state of the network, and the strongest coupling that may still allow for the mean pulse rate of the nodes in the network to remain bounded, respectively, in the large-network limit. In addition, we first derive a linear lower bound on the dependence of the nodes' pulse rate on the node degree, which implies that this dependence cannot exhibit sublinear asymptotic behavior at large node degrees in any pulse-coupled network.

### A. Lower bound on pulse rates

One iteration of Eq. (13) reveals a lower bound on the asymptotic pulse rate $m_k$, which is

$$m_k \geqslant \psi(1 + \lambda k). \tag{49}$$

A detailed derivation is presented in Appendix D. The meaning of the inequality in Eq. (49) is that the pulse rate of any $k$ node must equal or exceed its part stemming from the external drive and monosynaptic interactions mediating the external drive alone. Note that the estimate (49) prevents sublinear growth of the pulse rate $m_k$ with the node degree $k$.

### B. Sufficient estimate for bounded pulse rates

The scaling found for uncorrelated networks in Sec. IV B guarantees the existence of a stable, nonvanishing, steady state of the network in a larger class of networks, which we can characterize as *boundedly correlated*. [The expression originates from *degree-correlation* distribution, which is used synonymously with *edge-type* distribution for $T(n,k)$.] In this network class, the node degree and edge-type distributions, $P_{\text{in}}(n)$ and $T(n,k)$, must satisfy the condition

$$\frac{\mu^2 T(n,k)}{k P_{\text{in}}(k) n P_{\text{in}}(n)} \leqslant \eta \tag{50}$$

for some constant $\eta \geqslant 1$, independent of all incoming degree values, $k$ and $n$, and all network sizes, $N$. The fact that only the inequality $\eta \geqslant 1$ is admissible is seen easily if we multiply the inequality (50) by the denominator of its right-hand side and integrate over the node degrees $k$ and $n$. Recall that $\eta = 1$ corresponds to an uncorrelated network.

As we derive in Appendix D, condition (50) implies that the sum of the Liouville-Neumann series (15) for the pulse rate $m_k$ can be bounded by

$$m_k \leqslant \psi \left\{ 1 + k\lambda \left[ 1 + \eta \left( \frac{1}{1 - \lambda\eta \langle n^2 \rangle_N / \mu} - 1 \right) \right] \right\}, \tag{51}$$

which shows that scaling the coupling coefficient $\lambda$ by an $O(\mu/\eta\langle n^2\rangle_N)$ quantity will ensure that $m_k$ is finite over an entire $\lambda$ interval in the $N \gg 1$ limit. Moreover, for the network-averaged pulse rate, $\bar{m}$, the node degree $k$ is replaced with the mean node degree $\mu$ in the estimate (51), and since $\langle n^2\rangle_N \geqslant \mu^2$, this rate will also be finite under the above scaling.

Note that the networks in Secs. IV B–IV D are all boundedly correlated. Nevertheless, only for the uncorrelated network in Sec. IV B must the coupling parameter $\lambda$ be scaled by the ratio $\mu/\langle n^2\rangle_N$ in order to ensure finite pulse rates along an interval of $\lambda$ in the infinite-network limit. For the scale-free network in Sec. IV C, $\lambda$ only has to be scaled by a much larger quantity of $O(1/\langle n^2\rangle_N^{1/2})$, and for the unidirectional scale-free network in Sec. IV D, it need not be scaled at all. This shows that scaling $\lambda$ by a factor of size $O(\mu/\langle n^2\rangle_N)$ is sufficient to ensure finite pulse rates in the $N \gg 1$ limit along an interval of $\lambda$ for boundedly correlated networks, but not necessary. In addition, the uncorrelated network in Sec. IV B shows that this scaling must be used and thus is necessary for at least one network.

We now combine the estimates in Eqs. (49) and (51) and use the rescaling

$$\Lambda = \frac{\lambda\langle n^2\rangle_N}{\mu}, \quad \kappa = \frac{k\mu}{\langle n^2\rangle_N}, \tag{52}$$

to parametrize the gain curves. From this parametrization, in a boundedly correlated network, we see that for fixed external drive $\psi$ the curves representing the dependence of the pulse rate $m$ on the rescaled degree $\kappa$ reside in the wedge between the lines

$$m = \psi(1 + \kappa\Lambda)$$

and

$$m = \psi \left\{ 1 + \kappa\Lambda \left[ 1 + \frac{\eta^2\Lambda}{1 - \eta\Lambda} \right] \right\}$$

that is contained in the first quadrant, provided $\Lambda < 1/\eta$, regardless of the network size. This geometric consideration shows that the (average) growth of the pulse rate $m_k$ with the node degree $k$ can only be linear in this case. If $m_k$ is monotonically increasing in a boundedly correlated network, this growth must, in fact, be asymptotically linear in $k$, with the slope bounded by the corresponding coefficients in the inequalities (49) and (51) with the scaled coupling $\Lambda$ replacing $\lambda$.

Note that the estimate (51) only holds for coupling values $\lambda < \mu/\eta\langle n^2\rangle_N$. At $\lambda = \mu/\eta\langle n^2\rangle_N$ the right-hand side of Eq. (51) becomes infinite. For $\lambda > \mu/\eta\langle n^2\rangle_N$, the argument leading to Eq. (51) is invalid, and so (51) ceases to provide a valid estimate. Nevertheless, for some boundedly correlated networks, the firing rates $m_k$ may still remain bounded even for such large coupling values, and in fact superlinear growth of

$m_k$ may be permitted in this case. An example is the network discussed in Sec. IV D.

### C. Necessary estimate for bounded mean network pulse rate

The scaling found in Sec. IV C can be generalized to *statistically symmetric* networks, that is, those for which the expected outgoing degree of a node equals its incoming degree. In particular, if the function $P_{\text{out|in}}(l \mid n)$ denotes the probability for the outgoing degree of a given $n$ node in such a network to be $l$, then this node's expected outgoing degree must equal

$$\int_0^N l\, P_{\text{out|in}}(l \mid n) dl = n. \tag{53}$$

For networks with the property (53), the analog of the relation in Eq. (1) holds when we integrate over the incoming degree of the postsynaptic node, $k$, rather than over the incoming degree of the presynaptic node, $n$. This relation is the proportionality

$$\int_0^N T(n,k)dk \propto P_{\text{in}}(n) \int_0^N l\, P_{\text{out|in}}(l \mid n) dl, \tag{54}$$

with the integral on the left-hand side corresponding to the probability of a randomly chosen edge to originate at an $n$ node and the right-hand side stating that this probability is given by the probability of finding an $n$ node in the network multiplied by the expected number of edges originating at an $n$ node. After taking into account Eq. (53) and normalization, Eq. (54) becomes

$$\int_0^N T(n,k)dk = \frac{n P_{\text{in}}(n)}{\mu}. \tag{55}$$

In Appendix D we show that, for such statistically symmetric networks, iterating the integral equation in Eq. (13) twice and averaging it over the node-degree distribution $P_{\text{in}}(n)$ yields the estimate

$$\bar{m} = \psi + \psi\lambda\mu + \psi\lambda^2\langle n^2\rangle_N + O(\lambda^3), \tag{56}$$

where the $O(\lambda^3)$ term is non-negative. Consequently, for the average pulse rate $\bar{m}$ to remain bounded as the network size $N$ increases without a bound, it is necessary that at least the second and third terms on the right-hand side of Eq. (56) remain bounded. The third term will remain bounded if the network coupling parameter $\lambda$ scales as $O(1/\langle n^2\rangle_N^{1/2})$. Since $\langle n^2\rangle_N > \mu^2$, the second term on the right-hand side of Eq. (56) will also be bounded under this scaling.

For any network that is both boundedly correlated and statistically symmetric, the above estimates imply that the scaling of its coupling coefficient $\lambda$ must fall somewhere in the range

$$O(\mu/\langle n^2\rangle_N) \lesssim \lambda \lesssim O\left(1/\langle n^2\rangle_N^{1/2}\right) \tag{57}$$

for there to be a finite-size $\lambda$ interval on which the network has a stable, steady regime with finite pulse rates. The scale-free network in Sec. IV C is both statistically symmetric and boundedly correlated. We should note that the $O(1/\langle n^2\rangle_N^{1/2})$-scaling suffices to keep its pulse rates bounded within a finite interval of the coupling parameter for this network. Therefore, this largest possible scaling, in fact, suffices for this particular network.

Unsurprisingly, for the all-to-all coupled network of size $N+1$, the node-degree average and second moment equal $\mu = N$ and $\langle n^2\rangle_N = N^2$, so that both of the above scaling estimates of the coupling constant $S$ equal the $O(1/N)$-scaling derived in Sec. IV A. On the other hand, in scale-free networks, $\mu$ stays finite and $\langle n^2\rangle_N$ grows with growing $N$, so that the ratio of the two extreme scalings in Eq. (57) becomes unbounded.

The network in Sec. IV D presents a threefold example that puts the results in this section in a sharper focus. First, it shows that the scaling of the coupling coefficient $\lambda$ by the ratio $\mu/\langle n^2\rangle_N$ is sufficient but by no means necessary for a boundedly correlated network to have stable, bounded pulse rates $m_k$ or mean pulse rate $\bar{m}$ in the large-$N$ limit. Second, the pulse rates $m_k$ exhibit superlinear growth in $k$ for finite $\lambda$, that is, for $\lambda > \mu/\langle n^2\rangle_N$, for which the estimate (51) is no longer valid, as described at the end of Sec. V B. Note, however, that $\gamma \to 1$ as $\lambda \to 0$, so that asymptotically the linear growth of $m_k$ in $k$, as enforced by the estimate (51), is restored if $\lambda$ is scaled to vanish as $N \to \infty$. Third, the example of the network in Sec. IV D shows that, in the absence of statistical symmetry, the coupling coefficient $\lambda$ does not need to be scaled by $1/\langle n^2\rangle_N^{1/2}$ in order for the mean network pulse rate $\bar{m}$ to remain finite with increasing $N$. In fact, we recall that if $\lambda$ is not scaled, there is a range of $\lambda$ values for which the mean pulse rate $\bar{m}$ remains finite. Note that this range is followed by a $\lambda$ interval in which all the pulse rates $m_k$ are finite but their mean, $\bar{m}$, is infinite.

## VI. PULSE-RATE DISTRIBUTION

One motivation for the present study is the desire to understand how the distribution of the nodes' pulse rates reflects the underlying network topology. The interpretation of the probability density function as the derivative of the cumulative probability distribution function, together with the chain rule, imply the formula for the distribution of the pulse rate

$$P(m) = P_{\text{in}}(k)\frac{dk}{dm} \tag{58}$$

in which the node degree $k$ is obtained from the corresponding pulse rate by inverting the dependence $m = m_k$.

For the networks in Secs. IV B and IV C, whose pulse rates $m_k$ depend on $k$ linearly in the form $m_k = \psi(1+\alpha k)$, with $\alpha = \alpha(N,\lambda)$, Eq. (58) yields the equation

$$P(m) = \frac{1}{\alpha\psi} P_{\text{in}}\left[\frac{1}{\alpha}\left(\frac{m}{\psi} - 1\right)\right], \tag{59}$$

with $\psi$ as in Eq. (12a). For the scale-free network in Sec. IV C, Eq. (59) implies the asymptotic relation

$$P(m) \sim \frac{\ell^2\lambda^2\psi^2}{2(1-\lambda\mu-\lambda^2\sigma^2)^2 m^3}, \quad m \gg 1, \tag{60}$$

with $\mu = \ell$ and $\sigma^2 = \langle n^2\rangle_N - \mu^2 = \ell^2[\ln(N/\ell) - 2]/2$ as in Eq. (31). In other words, the distribution (60) of the pulse rate $m$ over the network is scale-free, reflecting the underlying scale-free network topology.

Similarly, for the asymmetric network in Sec. IV D, Eqs. (42) and (58) yield the asymptotic relation

$$P(m) \propto m^{-2/\gamma-1}. \tag{61}$$

This relation implies a scale-free distribution of the pulse rates as long as $\lambda < 1$, that is, $\gamma < 2$. However, when $\lambda > 1$, that is, $\gamma > 2$, while the pulse-rate distribution $P(m)$ in Eq. (61) does follow a power law, it is not scale-free under the strict definition of the term because the exponent of the pulse rate exceeds $-2$, and so the mean pulse rate becomes unbounded in the large-network limit.

## VII. DISCUSSION

The question of how network activity reflects the underlying architectural connectivity of a given pulse-coupled network is important for the experimental determination of such networks' coupling architecture and ties in with the broader question of how to determine a network's architectural connectivity from an indicator of its *functional connectivity* [29–36,47]. Scale-free functional connectivity of brain networks [33,44] and hippocampal-slice networks [46] was recently observed using functional magnetic resonance, and a combination of two-photon imaging and electrophysiological measurements, respectively. While architectural connectivity of brain networks may be measured directly using diffusion magnetic resonance tractography imaging [34], methods for deducing architectural connectivity from functional connectivity, such as the neuron firing rate, are not yet well developed, and as a first step in that direction, one should at least understand the easier reverse relationship. Here we have studied it for three idealized IF networks by deriving the explicit dependence of a node's pulse rate on its incoming degree and the external drive. Interesting numerical examples of the types of IF networks that give rise to scale-free distributions of firing rates were presented in Ref. [56].

For the scale-free IF networks we have investigated, our mean-field approach and simulations show that their pulse rates reflect the underlying power-law architectural connectivity distribution. This appears to perhaps be a manifestation of an, as yet unexplored, universal phenomenon exhibited by a number of pulse-coupled-type networks with very different dynamical units. For example, for traffic of particles, such as vehicles or internet data, on networks [7,57–83], diffusion-type analysis of noninteracting particles [75,78] and simulations of interacting particles [64,77] both indicate scale-free distributions of the amount of traffic passing through the nodes on scale-free networks in the free-flowing regime. One thus might conjecture the existence of a limiting, asymptotic, coarse-grained description that would apply to nodes with high incoming degrees, and therefore high pulse-rates, independently of the detailed behavior of the underlying dynamical unit, in a large class of pulse-coupled networks. While ascertaining the existence of such a description and determining the class in which it is valid would be important, it is far outside the scope of this paper and will be relegated to future work.

As we show in Sec. IV D, in the large-network limit, even in networks with a finite expected node degree, the mean pulse rate per node may become unbounded if the network coupling becomes too strong. Nevertheless, this may not disqualify the IF network in question from being an adequate model of pulse-coupled dynamics as long as the individual pulse rates of the nodes and inputs to them remain bounded.

For both boundedly correlated, statistically symmetric IF networks of Secs. IV B and IV C, the gain curves depicting their mean pulse rates become singular at the same coupling strength as the gain curves of all the $k$-node pulse rates. An interesting question that arises is whether this is a universal phenomenon in this class of IF networks. In other words, in this IF network class, is it true that the network-averaged pulse rate can only become singular when at least one of the $k$-node pulse rates does? The answer is a trivial yes for finite networks, but in the infinite-size limit, it is unknown. The network of Sec. IV D is a counterexample to this claim for more general IF networks, as that network lacks statistical symmetry.

Finally, we would like to point out that, in this paper, we have addressed the statistical steady state of pulse-coupled IF networks in which the network pulse trains are *asynchronous* as reflected in the assumption that the total network output pulse train follows Poisson statistics. A special limit of such networks, in which the time scale of the $\alpha$-function describing the pulse shape becomes infinitely short and the response amplitude infinitely large, exhibits a strong tendency toward synchronous oscillations. During those oscillations, different nodes' activity variables rise independently in a random fashion under the external drive, but then all the nodes fire at once, with this pattern repeating at approximately regular time intervals. An analytical theory of these oscillations for all-to-all coupled networks was developed in Refs. [84,85]. We are in the process of developing an analogous theory for networks with complex architectural connectivity, which will be described in a companion paper [86].

## ACKNOWLEDGMENTS

The authors would like to thank P. R. Kramer, K. A. Newhall, A. V. Rangan, and D. Zhou for helpful discussions. M.S. was partly supported by NSF Grant No. DMS-0636358. G.K. was partly supported by NSF Grant No. DMS-0506287. D.C. was partly supported by NSF Grant No. DMS-1009575.

## APPENDIX A: DERIVATION OF THE MEAN-FIELD MODEL

In this Appendix, we describe a derivation of the mean-field approximation to the IF pulse-coupled network model, as given in Eq. (8), which we have used to describe the pulse rates of the interacting dynamical units in the body of the paper. Since this is a well-known mean-field neuronal network model [37–40,87–90], our derivation proceeds in the framework of, and uses the standard terminology from, the theory of neuronal networks. Thus, only in this appendix, we refer to the $k$ nodes also as $k$ neurons, to the activity variable $v^i(t)$ in Eq. (4) as the neuronal voltage or membrane potential, to the pulse train $G^i(t)$ in Eq. (5) as the neuronal conductance, and to the $k$ nodes' pulse rate $m_k$ as the $k$ neurons' firing rate. Nevertheless, the derivation, as well as all the findings in this paper, should be

applicable to all pulse-coupled networks that can be described by the conductance-based IF model.

We begin our derivation by adding to Eq. (4) for the neuronal membrane-potential dynamics another differential equation modeling the neuronal conductance dynamics. The simplest such equation is

$$\tau_g \frac{dG^i}{dt} = -G^i + f\sum_j \delta(t-t_{ij}) + S\sum_{\kappa_i}\sum_j \delta\left(t-t_j^{\kappa_i}\right), \tag{A1}$$

where $\delta(\cdot)$ denotes the Dirac $\delta$ function. We refer to the train of the $\delta$ functions on the right-hand side of this equation as the spike train arriving at the $i$th neuron. Equation (A1) yields the conductance in Eq. (5) with the $\alpha$-type function $G(t)$ of the form $G(t) = \Theta(t)e^{-t/\tau_g}/\tau_g$, where $\Theta(\cdot)$ is the Heaviside function and $\tau_g$ is the conductance time constant.

In our numerical simulations, we used $G(t)$ as in Eq. (6) for the conductance time course instead, in order to achieve second-order accuracy [49]. This choice of the $\alpha$ function requires a second-order system instead of Eq. (A1); however, the final mean-field description turns out to be the same as for the network using Eq. (A1). For clarity of explanation, we therefore use Eq. (A1) to describe the network conductances.

We derive the mean-field description (8) of the network (4), (A1) using tools from nonequilibrium statistical mechanics, in particular, kinetic theory [37,38,91–107]. In what follows, we first derive a Fokker-Planck equation that gives the statistical description of the membrane potentials and conductances of the $k$ neurons and then derive the mean-field model (8) from this equation in the limit of vanishing input fluctuations.

### 1. Fokker-Planck equation

To investigate the statistical behavior of the network (4) and (A1), we employ a statistical ensemble composed of many copies of this network that are identical in every aspect except their initial voltages $V_i(0)$ and conductances $G_i(0)$, $i = 1,\ldots,N+1$, and their external inputs. Each input is an independent set of $N+1$ independent realizations of the Poisson spike train with the same rate $\nu(t)$, with each realization driving a different neuron.

We coarse-grain the neurons in the network according to their incoming degree and study the probability that, at time $t$, the membrane potential and conductance of a neuron with incoming degree $k$ lie in the rectangle with sides $(v,v+dv)$ and $(g,g+dg)$ in the $(v,g)$ phase space. This probability is given as $\rho_k(v,g,t)dvdg$, where $\rho_k(v,g,t)$ is the corresponding probability density function. Within the time interval $(t,t+dt)$, this probability changes due to (i) the smooth streaming of phase points through the sides of this rectangle, governed by the dynamics of Eqs. (4) and (A1) in the absence of spikes, and (ii) the spike-induced jumps in the neuronal conductance, governed by the sums of the Dirac $\delta$ functions in Eq. (A1).

Equations (4) and (A1) imply that, to the lowest order in $dv$, $dg$, and $dt$, the smooth streaming through the sides of the rectangle adds the change

$$\left\{\left[\left(\frac{v+dv-V_r}{\tau}\right)+g\left(\frac{v+dv-V_E}{\tau}\right)\right]\rho_k(v+dv,g,t) - \left[\left(\frac{v-V_r}{\tau}\right)+g\left(\frac{v-V_E}{\tau}\right)\right]\rho_k(v,g,t)\right\}dgdt + \left[\frac{g+dg}{\tau_g}\rho_k(v,g+dg,t)-\frac{g}{\tau_g}\rho_k(v,g,t)\right]dvdt. \tag{A2a}$$

The jumps induced by the external spikes add the change

$$\left[\rho_k\left(v,g-\frac{f}{\tau_g},t\right)-\rho_k(v,g,t)\right]dvdgdt \tag{A2b}$$

at the time rate $\nu(t)$, and those due to the network spikes the change

$$\left[\rho_k\left(v,g-\frac{S}{\tau_g},t\right)-\rho_k(v,g,t)\right]dvdgdt \tag{A2c}$$

at the time rate $k\mu_k(t)$, where $\mu_k(t)$ in Eq. (8c) is the average firing rate of a neuron that is presynaptic to a $k$ neuron.

It is important that the spike trains arriving at a given neuron obey Poisson statistics, so that the probability of a spike arrival over the time $dt$ indeed equals the product of the respective spike rate and $dt$. This is true for the external-drive train by assumption, but need not be true for the train arriving from the network. In particular, the spike train generated by any given neuron typically does not obey Poisson statistics. Only the joint output of many network neurons obeys these statistics asymptotically and provided that each neuron fires at a low rate and its spike times are mutually statistically independent [108]. Therefore, only spike trains arriving at $k$ neurons with high input-degree $k$ can be assumed as approximately Poisson, and the equations for the densities $\rho_k(v,g,t)$ with low node degrees $k$ are less accurate than those for the densities with high node-degrees under this assumption.

To derive the total change, $d\rho_k(v,g,t)\,dvdg$, of the probability density function $\rho_k(v,g,t)$ during the time interval $(t,t+dt)$, we add all the terms in Eq. (A2), with the terms in Eqs. (A2b) and (A2c) multiplied by their corresponding time rates. Dividing the resulting equation by the product of differentials, $dvdgdt$, in the limit as $dv\to 0$, $dg\to 0$ and $dt\to 0$, we find that the evolution of the probability density $\rho_k \equiv \rho_k(v,g,t)$, corresponding to $k$ neurons, is governed by the Boltzmann equation

$$\partial_t\rho_k = \partial_v\left\{\left[\left(\frac{v-V_r}{\tau}\right)+g\left(\frac{v-V_E}{\tau}\right)\right]\rho_k\right\} + \partial_g\left(\frac{g}{\tau_g}\rho_k\right) + \nu(t)\left[\rho_k\left(v,g-\frac{f}{\tau_g},t\right)-\rho_k(v,g,t)\right] + k\mu_k(t)\left[\rho_k\left(v,g-\frac{S}{\tau_g},t\right)-\rho_k(v,g,t)\right], \tag{A3a}$$

defined on the semi-infinite strip $V_r < v < V_T$, $0 < g < \infty$.

In Eq. (A3), the conductance jumps are accounted for by the terms on the last two lines of Eq. (A3a). If we assume the jumps to be small, we can Taylor expand the corresponding

jump terms to second order and derive the Fokker-Planck-type equation

$$\partial_t \rho_k = \partial_v \left\{ \left[ \left( \frac{v - V_r}{\tau} \right) + g \left( \frac{v - V_E}{\tau} \right) \right] \rho_k \right\} + \partial_g \left[ \frac{1}{\tau_g} (g - g_k(t)) \rho_k + \frac{\sigma_k^2(t)}{\tau_g} \partial_g \rho_k \right], \quad \text{(A4)}$$

where

$$g_k(t) = f\nu(t) + Sk\mu_k(t) \quad \text{(A5a)}$$

is the mean input to a $k$ neuron, and

$$\sigma_k^2(t) = \frac{1}{2\tau_g} [f^2 \nu(t) + S^2 k \mu_k(t)] \quad \text{(A5b)}$$

represents this neuron's variance of the input fluctuations. This equation is again defined on the semi-infinite strip $V_r \leqslant v < V_T$, $0 \leqslant g < \infty$.

We recast Eq. (A4) in the conservation form

$$\partial_t \rho_k(v,g,t) + \partial_v J_k^V(v,g,t) + \partial_g J_k^G(v,g,t) = 0, \quad \text{(A6)}$$

with the membrane-potential and conductance probability fluxes, $J_k^V$ and $J_k^G$, defined in the obvious way, and recall that when a neuron's membrane potential crosses the threshold $V_T$, it is reset to $V_r$ instantaneously, without changing the value of the conductance. From these two pieces of information we deduce the boundary condition connecting the membrane potential fluxes through the threshold $V_T$ and reset $V_r$,

$$J_k^V(V_T,g,t) = J_k^V(V_r,g,t), \quad \text{(A7a)}$$

for $0 \leqslant g < \infty$. Moreover, no negative or infinite neuronal conductance values can exist. Therefore, $\rho_k(v, g < 0, t) \equiv 0$ and

$$\rho_k(v, g \to \infty, t) \sim 0, \quad \text{(A7b)}$$

together with all its derivatives. Consequently, the conductance flux $J_k^G$ must vanish at $g = 0$, and $g = \infty$, so that

$$J_k^G(v, g = 0, t) = 0, \quad J_k^G(v, g \to \infty, t) = 0, \quad \text{(A7c)}$$

for $V_r \leqslant v < V_T$. Finally, the average firing rate of a $k$ neuron, $m_k(t)$, equals the integral of the probability flux $J_k^V(V_T,g,t)$ across the threshold over all the conductance values; that is,

$$m_k(t) = \int_0^\infty J_k^V(V_T,g,t)\, dg = -\int_0^\infty \left[ \left( \frac{V_T - V_r}{\tau} \right) + g \left( \frac{V_T - V_E}{\tau} \right) \right] \rho_k(V_T,g,t)\, dg. \quad \text{(A7d)}$$

Equation (A4), together with the boundary conditions (A7a)–(A7c) and the nonlinear self-consistency conditions (A7d), give the complete formulation of a Fokker-Planck-type kinetic theory for describing the neuronal network (4) and (A1) as an infinite system of partial differential equations for the densities $\rho_k(v,g,t)$. These equations are coupled nonlinearly through the coefficients (A5a) and (A5b), which couple through Eq. (8c) all the firing rates obtained from the boundary terms expressed in Eq. (A7d). The main task of the next section is to reduce this kinetic theory to the much simpler mean-field approximation in Eq. (8a) for the average firing rates $m_k$ of the $k$ neurons alone.

### 2. Mean-field approximation

We now address the mean-driven operating regime of the network (4) and (A1), in which the input fluctuations of any neuron become negligible as compared to its mean input, that is, $\sigma_k^2(t)/g_k(t) \to 0$ for the quantities in Eq. (A5) and all node degrees $k$. In this limiting network, the input to all $k$ neurons is the same, and the effect of the the last two terms in Eq. (A1) is statistically equivalent to a smooth input of the form $g_k(t) = f\nu(t) + Sk\mu_k(t)$. As can be deduced from Eqs. (4) and (A1) with this replacement, neuronal membrane potentials in this limit grow rapidly from reset to threshold and then fire. Therefore, in a statistical sense, information about a given neuron's instantaneous conductance value provides little information about its current membrane-potential value, and so one should expect that the dynamics of conductance and voltage are uncorrelated in this mean-driven limit.

In view of the discussion in the previous paragraph, in the mean-driven limit of Eq. (A4), we can therefore first assume the diffusion terms, which are multiplied by the conductance-fluctuations variance, $\sigma_k^2(t)$ in Eq. (A5b), to become negligible as compared to the rest of the terms in Eq. (A4). Second, we can also assume the probability densities of conductance and voltage to be statistically independent [38], so that

$$\rho_k(v,g,t) = \rho_k^{(v)}(v,t)\rho_k^{(g)}(g,t). \quad \text{(A8)}$$

Inserting the solution form (A8) into the resulting limit of Eq. (A4), integrating over the conductance, and taking into account the boundary condition (A7c), yields the equation

$$\partial_t \rho_k^{(v)}(v,t) = \partial_v \left\{ \left[ \left( \frac{v - V_r}{\tau} \right) + \langle g \rangle_k(t) \left( \frac{v - V_E}{\tau} \right) \right] \rho^{(v)}(v,t) \right\}, \quad \text{(A9a)}$$

where

$$\langle g \rangle_k(t) = \int_0^\infty g \rho_k^{(g)}(g,t) dg$$

is the expected conductance value. Likewise, inserting the solution form (A8) in the mean-driven limit of Eq. (A4), multiplying by the conductance, integrating over both the membrane potential and conductance, and taking into account the boundary condition (A7a) yields the equation

$$\frac{d}{dt} \langle g \rangle_k(t) = -\frac{1}{\tau_g} [\langle g \rangle_k(t) - g_k(t)] \quad \text{(A9b)}$$

for the expected conductance $\langle g \rangle_k(t)$, where $g_k(t) = f\nu(t) + Sk\mu_k(t)$ is the mean input to a $k$ neuron, given in Eq. (A5a). The boundary condition (A7d) translates into

$$m_k(t) = -\left[ \left( \frac{V_T - V_r}{\tau} \right) + \langle g \rangle_k(t) \left( \frac{V_T - V_E}{\tau} \right) \right] \rho_k^{(v)}(V_T,t). \quad \text{(A9c)}$$

In the stationary case, Eq. (A9b) relaxes to $\langle g\rangle_k = g_k = f\nu + S\mu_k$, and Eq. (A9a) can be integrated to yield

$$\rho_k^{(v)}(v) = -\frac{\tau m_k}{(v - V_r) + g_k(v - V_E)}. \tag{A10}$$

The normalization condition of $\rho_k^{(v)}(v)$ as a probability density function then gives the implicit equation for the firing rate $m_k$, Eq. (8a).

We now take a more careful look at the conditions that ensure the validity and consistency of the mean-field approximation. Intuitively, small input fluctuations should occur in neurons that receive many spikes, each of which induces a very small conductance jump. This is ensured by the limit in which $f \to 0$ and $S \to 0$ on the one hand, and at least one of $\nu \to \infty$ or $k\mu_k \to \infty$ on the other, but such that at least one of the products $f\nu$ and $Sk\mu_k$ remains bounded away from zero. An examination of the mean input $g_k$ and its variance $\sigma_k^2$ in Eqs. (A5) reveals that the ratio $\sigma_k^2/g_k$ indeed vanishes in this limit. Note that the rescalings of the coupling strength $S$ by factors that decay with the network size $N$ in Secs. IV and V ensure the limit $S \to 0$, and also that then, in fact, $\sigma_k^2/g_k \to 0$ regardless of whether $k\mu_k \to \infty$, remains bounded, or vanishes. Namely, in the latter two cases, the relative smallness of the input fluctuations is due to the external drive rather than the network drive.

For the network in Sec. IV D, however, the coupling strength $S$ does not need to be scaled so that it decays in the large-network limit, and thus there is no *a priori* reason why the mean-field model should even be applicable to it. Nevertheless, comparison with numerical simulations depicted in Fig. 5 clearly shows that the mean-field approximation is quite accurate for this network, and therefore we included it in the present paper. Why the validity of the mean-field model in this case extends well beyond its formal range appears still to be an open question, which will be addressed elsewhere.

## APPENDIX B: DERIVATION OF THE EDGE-TYPE DISTRIBUTION FUNCTION IN THE SCALE-FREE NETWORK

In this Appendix, we describe the derivation of the edge-distribution function, $T(n,k)$ in Eq. (32), associated with the pulse-coupled network studied in Sec. IV C. We construct this directed network in two steps: First we construct the corresponding undirected network following the algorithm described in Ref. [41], and then randomly assign a direction to each of the undirected edges.

In the major part of this Appendix, we discuss the calculation of the edge-distribution function, $T_u(n,k)$, in the undirected network of [41]. Therefore, in what is to follow, we use the term "degree of a node" to denote this node's *total degree*, that is, the number of all the (undirected) edges that emanate from this node. This use of the term "node degree" is restricted to this appendix only, as is the notation $P_u(k)$ for the distribution of these degrees and $T_u(n,k)$ for the the distribution of the edge types.

We grow the undirected network of [41] in stages: We begin with an all-to-all connected network consisting of $\ell$ nodes, which are said to be *active*. In addition, in order to avoid repeated node degrees, we modify the algorithm of [41] by also attaching the $j$th of these initial active $\ell$ nodes to precisely $j$ *inactive* nodes with degree 1. At each stage of the network growth, a new active node is attached to every active node via an undirected edge, resulting in $\ell + 1$ all-to-all connected, active nodes. At this point, one of the active nodes is *deactivated*; a node with the current degree $n$ is deactivated with the probability $\propto 1/n$. Once a node has been deactivated, it can never become active again. The procedure is repeated for each new node.

The network construction proceeds so that there are no repeated degrees in the set of active nodes at any stage of the network growth, as mentioned above, which can easily be shown by induction. In particular, if we begin with a set of $\ell$ active nodes with different degrees, all of which exceed or equal $\ell$, then upon adding a new node, we increase those degrees by one and end up with another set of $\ell$ nodes with all different degrees exceeding $\ell$, plus a node of degree $\ell$. After one of these $\ell + 1$ nodes is deactivated, we are back to $\ell$ nodes with all different degrees that exceed or equal $\ell$. Thus, except for the initial inactive nodes with degree 1, for every node in the network, its degree $n$ exceeds or equals the initial number of active nodes, $\ell$, that is, $n \geqslant \ell$. Note that the initial inactive nodes are not involved in the network construction and can be dropped at the end of it.

### 1. Master equation

We now construct a set of master equations to describe the expected number of edges connecting two deactivated nodes with degrees $n$ and $k$ after $t$ growth stages, denoted by $C_3(n,k,t)$, from whose large-$t$ limit we will compute the edge-type distribution $T_u(n,k)$. The following quantities are auxiliary in the computation of $C_3(n,k,t)$: (i) $P(n,t)$, the probability that an active node, randomly chosen after stage $t$, is an $n$ node; (ii) $C_1(n,k,t)$, the expected number of edges connecting nodes with degrees $n$ and $k$, with both nodes active after stage $t$; (iii) $C_2(n,k,t)$, the expected number of edges connecting nodes with degrees $n$ and $k$, with the node with degree $n$ deactivated and the node with degree $k$ active after stage $t$. Recall that all the node degrees involved in the construction exceed or equal the initial number of active nodes, $n,k \geqslant \ell$.

In order to construct the equations governing the evolution of the probability $P(n,t)$, $n > \ell$, we note that the expected number of active $n$ nodes after the $t$th node has been attached to the active nodes, but before one of these nodes is deactivated, is $\ell P(n-1,t-1)$. (Here we recall that $\ell$ is the number of active nodes before the new node has been attached; the expected number of nodes with degree $\ell$ is 1; that is, we are guaranteed the presence of the new node whose degree is $\ell$.) At the same time, according to the above rules of the network growth, there can be at most one active $n$ node at any growth stage, and therefore $\ell P(n-1,t-1)$ also must equal the probability, Prob($F$), of the event $F$ that one of the active nodes has degree $n$:

$$\ell P(n-1,t-1) = 1 \times \mathrm{Prob}(F) + 0 \times [1 - \mathrm{Prob}(F)] = \mathrm{Prob}(F). \tag{B1}$$

At the end of the stage $t$, one of the $\ell + 1$ nodes is deactivated. Let us introduce an auxiliary quantity, $\rho(n,t)$,

the probability that an active $n$ node is deactivated at the completion of stage $t$. [As mentioned above, $\rho(n,t) \propto 1/n$.] We then obtain the expression for the expected number of active $n$ nodes:

$$\ell P(n,t) = 1 \times [1 - \rho(n,t)]\,\mathrm{Prob}(F) + 0 \times \rho(n,t)\,\mathrm{Prob}(F) + 0 \times \mathrm{Prob}(F^c), \quad \text{(B2)}$$

where the superscript $c$ denotes the complement of the given event. In other words, upon the completion of the $t$th stage, the expected number of $n$ nodes is proportional to the expected number of $(n-1)$ nodes at the $(t-1)$st stage. From Eqs. (B1) and (B2), we thus find that $P(n,t)$ evolves according to the equation

$$P(n,t) = P(n-1,t-1)[1 - \rho(n,t)]. \quad \text{(B3a)}$$

To find the expression for the above probability $\rho(n,t)$, we count, as above, the expected number of active $n$ nodes by $\ell P(n-1,t-1)$, $n > \ell$. Realizing that the last added active node is certain to be the only one with degree $\ell$, and neglecting the certainty that the deactivated $n$ node was among the active nodes, we find the approximate normalization factor in $\rho(n,t)$. Thus, we derive for $\rho(n,t)$ the approximate formula

$$\rho(n,t) = \frac{1}{n\left(\ell \sum_{i=\ell+1}^{t+2\ell-1} P(i-1,t-1)/i + 1/\ell\right)}. \quad \text{(B3b)}$$

Using a similar argument, we can show that the evolution of the number of edges linking two active nodes with degrees $n$ and $k$, $C_1(n,k,t)$, is governed by the equation

$$C_1(n,k,t) = C_1(n-1,k-1,t-1)[1 - \rho(n,t) - \rho(k,t)], \quad \text{(B3c)}$$

where the factor $C_1(n-1,k-1,t-1)$ corresponds to the number of edges connecting nodes with degrees $n$ and $k$ during the $t$th stage, before the next node is deactivated, and the factor in the brackets is the probability that neither of the two nodes is deactivated at this stage.

The evolution of the number of edges linking an active node with degree $k$ and an inactive node with degree $n$, $C_2(n,k,t)$, is governed by the equation

$$C_2(n,k,t) = C_2(n,k-1,t-1)[1 - \rho(k,t)] + C_1(n-1,k-1,t-1)\rho(n,t). \quad \text{(B3d)}$$

In the first term of the sum on the right-hand side, the factor $C_2(n,k-1,t-1)$ corresponds to the number of edges connecting an inactive node with degree $n$ and an active node with degree $k$ during the $t$th stage before the next node is deactivated, and the factor in the square brackets gives the probability that the active node of degree $k$ is not deactivated at this stage. The second term corresponds to the expected number of edges that connected two active nodes with degrees $n-1$ and $k-1$ at stage $t-1$, where the node with degree $n-1$ was deactivated immediately after receiving an additional edge from the newly added node.

Finally, the evolution of the number of edges linking two inactive nodes with degrees $n$ and $k$, $C_3(n,k,t)$, is governed by the equation

$$C_3(n,k,t) = C_3(n,k,t-1) + C_2(n,k-1,t-1)\rho(k,t) + C_2(k,n-1,t-1)\rho(n,t). \quad \text{(B3e)}$$

The first term on the right-hand side of Eq. (B3e) gives the number of edges connecting two inactive nodes at stage $t-1$. This number is updated during the subsequent stage by an edge connecting what at stage $t-1$ were an inactive node with degree $n$ and an active node with degree $k-1$, or vice versa, with either active node being deactivated during stage $t$ with probability $\rho(k,t)$ or $\rho(n,t)$, respectively, after receiving an additional edge from the newly added node.

The *nonvanishing* initial conditions for the quantities in Eqs. (B3) are

$$P(n,0) = 1/\ell, \quad \text{when} \quad n \in [\ell, 2\ell-1], \quad \text{(B4a)}$$

$$C_1(n,k,0) = 1, \quad \text{when} \quad n,k \in [\ell, 2\ell-1], \quad n \neq k, \quad \text{(B4b)}$$

$$C_2(1,k,0) = k - \ell + 1, \quad \text{when} \quad k \in [\ell, 2\ell-1]; \quad \text{(B4c)}$$

all the other initial conditions vanish. These conditions correspond to the initial network with the $\ell$ all-to-all connected active nodes and the $\ell$ inactive nodes of degrees $1, \ldots, \ell$ connected to them.

The boundary conditions for Eqs. (B3) are

$$P(\ell,t) = [1 - \rho(\ell,t)]/\ell, \quad \text{(B5a)}$$

$$C_1(n,\ell,t) = C_1(\ell,n,t) = \ell P(n-1,t-1)[1 - \rho(n,t) - \rho(\ell,t)], \quad \text{(B5b)}$$

$$C_2(n,\ell,t) = \ell P(n-1,t-1)\rho(n,t), \quad \text{(B5c)}$$

$$C_2(\ell,n,t) = C_2(\ell,n-1,t-1)[1 - \rho(n,t)] + \ell P(n-1,t-1)\rho(\ell,t), \quad \text{(B5d)}$$

$$C_3(\ell,n,t) = C_3(n,\ell,t) = C_3(n,\ell,t-1) + C_2(\ell,n-1,t-1)\rho(n,t), \quad \text{if} \quad n \neq \ell, \quad \text{(B5e)}$$

$$C_3(\ell,\ell,t) = 0, \quad \text{(B5f)}$$

where $\rho(\cdot,t)$ can be computed from Eq. (B3b) using only quantities known from stage $t-1$. Arguments used to obtain these conditions are similar to those used in the derivation of the corresponding recurrence equations, except that the expected number of active $\ell$ nodes just before the completion of a stage always equals 1. Thus, the right-hand side of Eq. (B5a) equals the probability that an active node picked at random with probability $1/\ell$ will be the $\ell$ node, given that this node has not been deactivated. Likewise, the expected number of edges connecting an active node with degree $n$ to the sole active node with degree $\ell$ just before the $t$th stage is completed is now given by $\ell P(n-1,t-1)$ rather than by $C_1(n-1,k-1,t-1)$ used in Eqs. (B3c) and (B3d), which hold when both $n,k \geqslant (\ell+1)$. Equation (B5e) is obtained in the same manner as Eq. (B3e), except taking into account that no node with degree $< \ell$ exists, and so $C_2(n,\ell-1,t-1) = 0$. For the same reason, we must have $C_3(\ell,\ell,t) = C_3(\ell,\ell,t-1)$, and since $C_3(\ell,\ell,0) = 0$, Eq. (B5f) follows.

### 2. Late-stage asymptotics

We study the equations (B3a)–(B3e) in the limit of large $t$, in the approximation of continuous $n$ and $k$. In this limit, all the edges can be considered deactivated and their distribution is described by the function $C_3(n,k,t)$. The influence of the initial conditions becomes lost in this limit. We drop the argument $t$ in all the dependent variables except $C_3$, so that $P(n) \sim P(n,t \gg 1)$, $\rho(n) \sim \rho(n,t \gg 1)$, and $C_i(n,k) \sim C_i(n,k,t \gg 1)$, $i = 1,2$. Note that, in this limit, the network size grows without a bound, so that $t \to \infty$ implies $N \to \infty$. In the rest of this Appendix, we therefore assume that the network size $N$ is large and consistently neglect quantities that decay as $N$ grows.

#### a. $P$ and $\rho$ asymptotics

In the large-$t$ limit, after the probability density $\rho(n)$ is expressed through Eqs. (B3b) and (B3a) becomes

$$\frac{dP(n)}{dn} = -\frac{P(n)}{n\left[\ell \int_\ell^\infty P(k)dk/k + 1/\ell\right]}, \tag{B6}$$

where the difference $P(n) - P(n-1)$ has turned into the derivative with respect to $n$ and the sum in the denominator on the right-hand side has become an integral. The infinite upper limit is the result of the limit $t \to \infty$.

We look for a solution of Eq. (B6) in the form of $P(n) = \alpha n^\gamma$, $n \geqslant \ell$. From the normalization $\int_\ell^\infty P(n)\,dn = 1$ we find that

$$\alpha = -(\gamma+1)\ell^{-(\gamma+1)}. \tag{B7}$$

Substituting this $P(n)$ anzatz in Eq. (B6), we then find the value of $\gamma$ to be

$$\gamma = -\frac{2}{1+1/\ell}, \tag{B8}$$

which also implies that the denominator on the right-hand side of Eq. (B6) equals $-\gamma$. Further substituting this denominator in Eq. (B3b), we finally find the distribution $\rho(n)$ to be given by

$$\rho(n) = -\frac{\gamma}{n}. \tag{B9}$$

#### b. $C_1$ asymptotics

The asymptotic behavior of $C_1(n,k)$ is found by approximating Eq. (B3c) in the continuous limit of $n$ and $k$ with the partial differential equation

$$\frac{\partial C_1}{\partial n}(n,k) + \frac{\partial C_1}{\partial k}(n,k) = -C_1(n,k)[\rho(n)+\rho(k)] = \gamma C_1(n,k)\left(\frac{1}{n}+\frac{1}{k}\right), \tag{B10}$$

where we used Eq. (B9). Using the method of characteristics [109,110], we find the solution of this equation to be of the form

$$C_1(n,k) = \beta n^\gamma k^\gamma G(|n-k|), \tag{B11}$$

where the constant $\beta$ and the function $G(\cdot)$ are obtained from the boundary conditions (B5). Note, in particular, that there is never an edge connecting two active nodes with the same degree, therefore $C_1(n,n) = 0$, which we formally take into account by setting

$$G(|n-k|) = 1 - \delta(n-k). \tag{B12}$$

From the boundary conditions (B5b), we find

$$C_1(n,\ell) = \ell P(n)[1-\rho(n)-\rho(\ell)] = \alpha n^\gamma \ell\left(1+\frac{\gamma}{n}+\frac{\gamma}{\ell}\right). \tag{B13}$$

At the same time, from Eqs. (B11) and (B12), we find $C_1(n,\ell) = \beta n^\gamma \ell^\gamma$, and therefore for $n \geqslant \ell \gg 1$

$$\beta = \alpha \ell^{-\gamma+1} = -(\gamma+1)\ell^{-2\gamma} \tag{B14}$$

and

$$C_1(n,k) = -(\gamma+1)\ell^{-2\gamma} n^\gamma k^\gamma [1-\delta(n-k)]. \tag{B15}$$

#### c. $C_2$ asymptotics

Again, by treating $n$ and $k$ as continuous variables, we approximate the difference in Eq. (B3d) by

$$\frac{\partial C_2}{\partial k}(n,k) = -C_2(n,k)\rho(k) + C_1(n,k)\rho(n).$$

Using Eqs. (B9) and (B15), we can rewrite this equation as

$$\frac{\partial C_2}{\partial k}(n,k) - \frac{\gamma C_2(n,k)}{k} = -\gamma\beta n^{\gamma-1}k^\gamma[1-\delta(n-k)],$$

which, after being multiplied by $k^{-\gamma}$, reduces to

$$[k^{-\gamma}C_2(n,k)]_k = -\gamma\beta n^{\gamma-1}[1-\delta(n-k)].$$

Integrating this equation over $k$ and multiplying the result by $k^\gamma$, we obtain

$$C_2(n,k) = -\gamma\beta n^{\gamma-1}k^{\gamma+1} + \xi(n)k^\gamma + 2\gamma\beta n^{\gamma-1}k^\gamma H(n-k), \tag{B16}$$

where $H(\cdot)$ is the Heaviside function and $\xi(\cdot)$ is an unknown arbitrary function. Letting $k = \ell$ and $n \neq \ell$ in this equation, we find

$$C_2(n,\ell) = -\gamma\beta n^{\gamma-1}\ell^{\gamma+1} + \xi(n)\ell^\gamma,$$

while the boundary condition in Eq. (B5c) gives

$$C_2(n,\ell) = -\gamma\alpha\ell n^{\gamma-1},$$

which determines the unknown function as $\xi(n) = \varphi n^{\gamma-1}$, where $\varphi$ is given by the expression

$$\varphi = \ell^{-\gamma+1}\gamma(\beta\ell^\gamma - \alpha). \tag{B17}$$

Thus, the final expression for the number $C_2(n,k)$ is

$$C_2(n,k) = -\gamma\beta n^{\gamma-1}k^{\gamma+1} + \varphi n^{\gamma-1}k^\gamma + 2\gamma\beta n^{\gamma-1}k^\gamma H(n-k), \tag{B18}$$

where $\alpha$, $\beta$, and $\gamma$ are given by Eqs. (B7), (B14), and (B8), respectively.

#### d. $C_3$ asymptotics

Finally, for continuous $n$ and $k$ and $t \gg 1$, Eq. (B3e) for the function $C_3(n,k,t)$ is approximated by the equation

$$\frac{\partial C_3}{\partial t}(n,k,t) = C_2(n,k)\rho(k) + C_2(k,n)\rho(n),$$

where we have approximated $n \sim n-1$ and $k \sim k-1$, respectively. Integrating this equation over $t$ and using Eqs. (B9) and (B18), we find

$$\begin{aligned} C_3(n,k,t) &\sim t[C_2(n,k-1)\rho(k) + C_2(k,n-1)\rho(n)] \\ &= t\Bigg[n^{\gamma-1}(-\gamma\beta k^{\gamma+1} + \varphi k^{\gamma})\left(-\frac{\gamma}{k}\right) \\ &\quad + k^{\gamma-1}(-\gamma\beta n^{\gamma+1} + \varphi n^{\gamma})\left(-\frac{\gamma}{n}\right) \\ &\quad - 2\gamma^2\beta n^{\gamma-1}k^{\gamma-1}\Bigg], \end{aligned}$$

where the last term is the result of adding two Heaviside functions. This expression finally simplifies to

$$C_3(n,k,t) \sim t\gamma^2\beta(n^{\gamma-1}k^{\gamma} + n^{\gamma}k^{\gamma-1} - 2\ell k^{\gamma-1}n^{\gamma-1}), \quad \text{(B19)}$$

where the constants $\beta$ and $\gamma$ are given in Eqs. (B14) and (B8), respectively.

### 3. Large initial network approximation

For a large number, $\ell$, of initial active nodes, the parameter $\gamma$ in Eq. (B8) satisfies the relationship $\gamma \approx -2$. Therefore, in this limit, Eq. (B19) for the edge-distribution function $T_u(n,k)$ reduces to the equation

$$C_3(n,k,t) = t\gamma^2\beta\left(\frac{1}{n^3k^2} + \frac{1}{n^2k^3} - \frac{2\ell}{k^3n^3}\right). \quad \text{(B20)}$$

As shown in Ref. [41], the distribution of the node degrees for this network equals

$$P_u(k) = \frac{2\ell^2}{k^3}, \quad \text{(B21)}$$

with the mean degree $\mu_u \equiv 2\ell$. Therefore, the edge-distribution function, $T_u(n,k)$, which is obtained by normalizing the function $C_3(n,k)$, is given by the formula

$$T_u(n,k) = A\,P_u(n)P_u(k)(n+k-\mu_u), \quad \text{(B22)}$$

where the constant $A$ is obtained from the normalization of the function $T_u(n,k)$,

$$\begin{aligned} 1 &= \int_{\ell}^{\infty}\int_{\ell}^{\infty} T_u(n,k)\,dn\,dk \\ &= A\int_{\ell}^{\infty}\int_{\ell}^{\infty} P_u(n)P_u(k)(n+k-\mu_u)\,dn\,dk = A\mu_u. \end{aligned} \quad \text{(B23)}$$

We thus conclude that

$$T_u(n,k) = \frac{P_u(n)P_u(k)(n+k-\mu_u)}{\mu_u}, \quad \text{(B24)}$$

up to terms that decay with the network size.

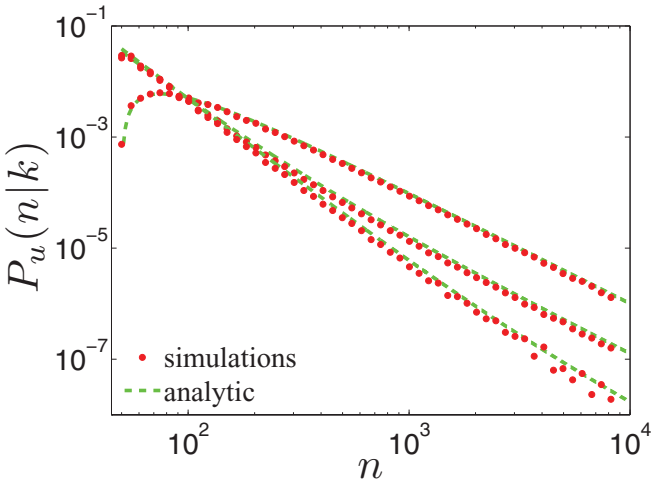


FIG. 8. (Color online) The dependence of the conditional probability $P_u(n\,|\,k)$ in the undirected network with $\ell = 50$, as derived from the edge-distribution function $T_u(n,k)$ and the incoming-degree distribution $P_u(k)$ using Eq. (3). The dots (red online) represent averages over $10^3$ network realizations using Monte Carlo simulations of the network of size $N = 10^4$. The dashed line (green online) represents the analytical result of Eqs. (B21) and (B24) with $n,k \geqslant \ell$. (Recall that $P_u(n\,|\,k) = 0$ for $n,k < \ell$.) Top to bottom on the right-hand side of the figure: $k = 50$, 400, and 4000.

We have verified the accuracy of the approximation in Eq. (B24) by comparing its results with those of direct numerical Monte Carlo simulations. The comparison is presented in Fig. 8, which shows a highly accurate match provided the expressions in Eqs. (B21) and (B24) are normalized using sums over integers rather than integrals. We present the conditional probability $P_u(n\,|\,k)$, as derived from the edge-distribution function $T_u(n,k)$ and the incoming-degree distribution $P_u(k)$ using Eq. (3), because the curves representing it are normalized and therefore easier to depict on one set of axes. Equation (3) holds for total degrees just as it holds for incoming degrees and for the same reason.

### 4. Directed network

Finally, we compute approximate expressions for the node-degree and edge-type distribution functions in the directed network from the corresponding distributions in the undirected network. We compute these approximate expressions in the limit of a large initial number of active nodes, $\ell \gg 1$. Recall that we obtain the directed network by assigning the direction to every edge in the undirected network randomly with probability 1/2.

#### a. The node-degree distribution

First, let us discuss how to obtain the incoming-degree distribution in the directed network, $P_{\text{in}}(k)$, from the total-degree distribution of the undirected network,

$$P_u(k) = \frac{2\ell^2}{k^3}, \quad \text{(B25)}$$

which was derived in Ref. [41]. We begin by determining the number of ways in which a given $n$ node in the undirected

network can become a $k$ node in the directed network, which equals $\binom{n}{k}$. [Recall that $\binom{n}{k} = 0$ if $k > n$.] The probability that an undirected edge emanating from this node becomes an incoming edge for this node is $1/2$, and the same for an outgoing edge. Therefore, the probability that an $n$ node in the undirected network can become a $k$ node in the directed network equals

$$\binom{n}{k}\left(\frac{1}{2}\right)^n.$$

Using the law of total probability, if all node degrees were allowed in the undirected network, we would find that the directed node-degree distribution $P_{\text{in}}(k)$ obtained from the undirected node-degree distribution $P_u(n)$ would be given by

$$P_{\text{in}}(k) = \sum_{n=k}^{N} \binom{n}{k}\left(\frac{1}{2}\right)^n P_u(n).$$

Since, in our case, the undirected network can only have nodes with degrees $\nu \geqslant \ell$, then

$$P_{\text{in}}(k) = \sum_{n=\max\{\ell,k\}}^{N} \binom{n}{k}\left(\frac{1}{2}\right)^n P_u(n). \tag{B26}$$

Note that we clearly can have $k < \ell$ in the directed network.

The De Moivre-Laplace theorem [111] shows that the binomial distribution can be approximated by the Gaussian distribution for large $n$ and $k - n/2 = O(\sqrt{n})$ as

$$\binom{n}{k}\left(\frac{1}{2}\right)^n \sim \frac{1}{\sqrt{\pi n/2}} \exp\left(-\frac{(k-n/2)^2}{n/2}\right). \tag{B27}$$

(For other values of $k$, both sides are exponentially small.) Using the undirected-network degree distribution (B25), we therefore find for the directed network distribution (B26) the approximate expression

$$P_{\text{in}}(k) \sim 2^{3/2}\pi^{-1/2}\ell^2 \times \int_{\max\{\ell,k\}}^{N} n^{-7/2} \exp\left(-\frac{(k-n/2)^2}{n/2}\right) dn, \tag{B28}$$

and the substitution $n = 2kv$ lets us transform this integral into the form

$$P_{\text{in}}(k) \sim 2^{-1}\pi^{-1/2}\ell^2 k^{-5/2} \times \int_{\max\{\ell/2k,1/2\}}^{N/2k} v^{-7/2} \exp\left(-k\,\frac{(1-v)^2}{v}\right) dv. \tag{B29}$$

For large values of $k$, the right-hand side of Eq. (B29) contains the type of integral whose asymptotic behavior can be calculated using Laplace's method by expanding around the maximum of the exponent at $v = 1$. The gist of this method is the realization that the exponential can be approximated beyond all orders by a Gaussian centered at the maximum of the exponent and that only an $O(1/\sqrt{k})$-size neighborhood of this maximum counts in the integration. Therefore, for $k > \ell/2$, we can move the lower limit of integration in Eq. (B29) to any fixed number below 1 while only incurring a negligible error at any order of the expansion. On the other hand, when $k \lesssim \ell/2$, the lower limit $\ell/2k$ must be retained. Therefore, at the leading order, we can fix the lower limit in Eq. (B29) at $\ell/2k$. Moreover, the $v$ variations in the powers multiplying the exponential can be ignored in both cases. Therefore, after making the coordinate change $x = v - 1$, we can approximate the integral in Eq. (B29) by

$$\begin{aligned} P_{\text{in}}(k) &\sim 2^{-1}\pi^{-1/2}\ell^2 k^{-5/2} \int_{\ell/2k-1}^{N/2k-1} \exp(-kx^2)dx \\ &= \frac{\ell^2}{4k^3}\left\{\operatorname{erf}\left[\sqrt{k}\left(\frac{N}{2k}-1\right)\right] - \operatorname{erf}\left[\sqrt{k}\left(\frac{\ell}{2k}-1\right)\right]\right\}, \end{aligned} \tag{B30}$$

where $\operatorname{erf}(\cdot)$ is the complementary error function $\operatorname{erf}(z) = (2/\sqrt{\pi})\int_0^z e^{-t^2}\,dt$.

For $1 \ll \ell/2 \ll k \ll N/2$ we find the final asymptotic approximation for the function in Eq. (B30) to be as in Eq. (30), while for $1 \ll k \lesssim \ell/2$ or $k \gtrsim N/2$ the function in Eq. (B30) has an $O(\sqrt{k})$-wide transition layer near $k = \ell/2$ or $k = N/2$, respectively. For $k = O(1) \ll \ell$, one must scale the integration variable in Eq. (B28) by $\ell$ instead of $k$ and perform a similar Laplace-type asymptotic analysis. However, the result of this analysis and Eq. (B30) both give $P_{\text{in}}(k)$, which is exponentially small in $\ell$ and thus negligible for $k = O(1) \ll \ell$. Therefore, using Eq. (B30) all the way down into this regime gives an acceptable uniform asymptotic approximation of the density $P_{\text{in}}(k)$. In fact, in view of the sharp transition in the density $P_{\text{in}}(k)$ near $k = \ell/2$ between the expression in Eq. (30) and an exponentially small quantity, we approximate $P_{\text{in}}(k)$ even more simply by Eq. (30) for nodes with incoming degrees $k \geqslant \ell/2$ and 0 for those with degrees $k < \ell/2$. Likewise, we approximate $P_{\text{in}}(k)$ as vanishing for $k > N/2$. This is the approximation that we use in the body of the paper.

#### *b. The edge-type distribution*

We use a similar procedure to approximate the edge-type distribution function in the directed network. The probability that an edge connecting a $\nu$ node to a $\kappa$ node in the undirected network becomes a directed edge connecting an $n$ node to a $k$ node in the directed network is computed as follows: First, let us assume that the $\nu$ node becomes the $n$ node and the $\kappa$ node becomes the $k$ node. Note that the probability is $1/2$ that the direction of the edge is chosen to point from the $\nu$ node to the $\kappa$ node. We therefore know that the $\nu$ node must acquire one outgoing edge and so must still get $n$ incoming edges chosen from the total of $\nu - 1$ undirected edges. Likewise, the $\kappa$ node must acquire one incoming edge, and so must still get $k - 1$ incoming edges from among $\kappa - 1$ undirected edges. Altogether, the number of ways this can be accomplished is thus

$$\binom{\nu-1}{n}\binom{\kappa-1}{k-1}$$

and the conditional probability for this to happen is

$$\binom{\nu-1}{n}\binom{\kappa-1}{k-1}\left(\frac{1}{2}\right)^{\nu+\kappa-2},$$

given that the direction of the edge was chosen from the $\nu$ node to the $\kappa$ node. The total probability for this to happen is therefore

$$\binom{\nu-1}{n}\binom{\kappa-1}{k-1}\left(\frac{1}{2}\right)^{\nu+\kappa-1}.$$

Likewise, if the $\nu$ node in the undirected network becomes the $k$ node in the directed network and the $\kappa$ node in the undirected network becomes the $n$ node in the directed network at the two ends of the given edge, the probability for this event is

$$\binom{\nu-1}{k-1}\binom{\kappa-1}{n}\left(\frac{1}{2}\right)^{\nu+\kappa-1}.$$

Therefore, altogether, the probability that an undirected edge connecting a $\nu$ node to a $\kappa$ node in the undirected network becomes a directed edge connecting an $n$ node to a $k$ node in the directed network is

$$\binom{\nu-1}{n}\binom{\kappa-1}{k-1}\left(\frac{1}{2}\right)^{\nu+\kappa-1} + \binom{\nu-1}{k-1}\binom{\kappa-1}{n}\left(\frac{1}{2}\right)^{\nu+\kappa-1}.$$

If all the node degrees in the undirected network were allowed, the expression for the distribution $T_d(n,k)$ would thus be

$$\begin{aligned} T_d(n,k) &= \sum_{\nu=n+1}^{N}\sum_{\kappa=k}^{N}\binom{\nu-1}{n}\binom{\kappa-1}{k-1}\left(\frac{1}{2}\right)^{\nu+\kappa-1} T_u(\nu,\kappa) \\ &\quad + \sum_{\nu=k}^{N}\sum_{\kappa=n+1}^{N}\binom{\nu-1}{k-1}\binom{\kappa-1}{n}\left(\frac{1}{2}\right)^{\nu+\kappa-1} T_u(\nu,\kappa) \\ &= \sum_{\nu=n+1}^{N}\sum_{\kappa=k}^{N}\binom{\nu-1}{n}\binom{\kappa-1}{k-1}\left(\frac{1}{2}\right)^{\nu+\kappa-2} T_u(\nu,\kappa), \end{aligned}$$

where we have taken into account that the distribution $T_u(\nu,\kappa)$ is symmetric with respect to interchanging its arguments. Since only degrees $\nu,\kappa \geqslant \ell$ are allowed in our undirected network, this formula becomes

$$T_d(n,k) = \sum_{\nu=\max\{\ell,n+1\}}^{N}\sum_{\kappa=\max\{\ell,k\}}^{N}\binom{\nu-1}{n} \times \binom{\kappa-1}{k-1}\left(\frac{1}{2}\right)^{\nu+\kappa-2} T_u(\nu,\kappa), \quad \text{(B31)}$$

To find the large-$\ell$ approximation for the edge-type distribution $T_d(n,k)$ in Eq. (B31), we again begin by approximating its coefficients using the DeMoivre-Laplace formula (B27), replacing the sums with appropriate integrals, and applying Laplace's method. While the calculation is considerably more involved than that leading to the directed edge distribution, the end result is indeed given by Eq. (32) for $\ell/2 < n,k < N/2$, and negligibly small otherwise. Instead of giving the details of this calculation, in Fig. 9, we show the agreement of this large-$\ell$ asymptotic approximation for $T_d(n,k)$ with the approximate evaluation of Eq. (B31), as described below, and

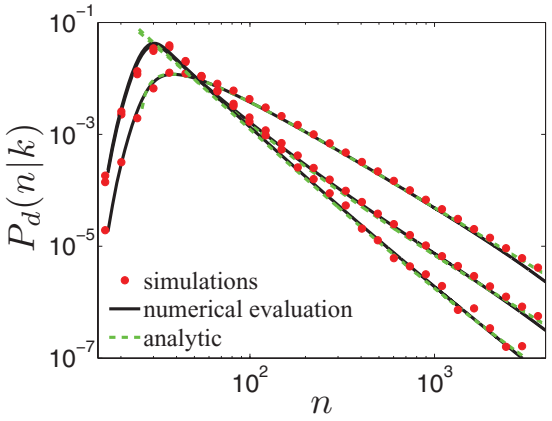


FIG. 9. (Color online) The dependence of the conditional probability $P_d(n\,|\,k)$ in the directed network with $\ell = 50$, as derived from the edge-distribution function $T_d(n,k)$ and the incoming-degree distribution $P_{\text{in}}(k)$ using Eq. (3). The dots (red online) represent averages over $10^3$ network realizations using Monte Carlo simulations of the network of size $N = 10^4$. The solid line (black online) represents a numerical evaluation using Eqs. (B31) and (B26) as described in the text. The dashed line (green online) represents the analytical result of Eqs. (30) and (32) with $\ell/2 < n,k < N/2$. Top to bottom on the right-hand side of the figure: $k = 25$, 200, and 2000. We do not display the transition layer near $n = N/2$.

the results of Monte Carlo simulations. For ease of depiction, we again present the conditional probability $P_d(n\,|\,k)$, as derived from the edge-distribution function $T_d(n,k)$ and the incoming-degree distribution $P_{\text{in}}(k)$ using Eq. (3).

Finally, for a directed network of size $N$, a direct numerical evaluation of the edge distribution $T_d(n,k)$ in Eq. (B31) would require $\sim N^4$ operations ($10^{16}$ in our case). Instead, for $\ell/2 \lesssim n,k \lesssim N/2$, we approximate the sums in Eq. (B31) by taking $\nu$'s and $\kappa$'s from the intervals centered at $2n$ and $2k$ with half-widths $2\sqrt{2n}$ and $2\sqrt{2k}$, respectively. These two half-widths approximately equal twice the standard deviations of the (approximately) binomial distributions appearing in Eq. (B31).

## APPENDIX C: LEADING-ORDER PULSE RATE FOR THE ASYMMETRIC, SCALE-FREE NETWORK

In this Appendix we derive Eq. (46) from Sec. IV D. We begin by seeking a solution of Eq. (13) with large-$k$ asymptotic behavior $m_k \sim Bk^{\gamma}$, where $\gamma > 1$, assumed in Eq. (45). Inserting this ansatz into Eq. (13) and computing the kernel $K(n,k)$ from Eqs. (14), (42), and (43), we arrive at integrals of the form

$$\int_0^{\infty}\frac{n^{\gamma}\,dn}{\prod_{j=r}^{l}(n+a_j)} = -\frac{\pi}{\sin\pi\gamma}\sum_{j=1}^{r}\frac{a_j^{\gamma}}{\prod_{\substack{l=1\\ l\neq j}}^{r}(a_l-a_j)}, \quad \text{(C1)}$$

with $a_j > 0$, $j = 1,\ldots,r$. These integrals are evaluated using residues over a keyhole contour, with the keyhole comprising the upper and lower edge of the branch cut along the positive real axis and a small circle around the origin, and the rest of the contour consisting of a large circle.

Using the result of Eq. (C1), which in our case converges for $\gamma < 4$, we find Eq. (13) to have become

$$\begin{aligned} Bk^\gamma \sim\ & \psi - \frac{\pi B\lambda}{\sin\pi\gamma}\Big\{k+3-2^\gamma(k+1) \\ & -\frac{1}{2}[(k+1)^{\gamma+1}(k+2)(k+3) \\ & -(k+2)^{\gamma+1}(k+3)(3k+1) \\ & +(k+3)^{\gamma+1}k(3k+5) \\ & -(k+4)^\gamma k(k+1)(k+3)]\Big\}. \end{aligned} \tag{C2}$$

Expanding the expression on the right-hand side of this equation for large values of $k$, we find that the $O(k^{\gamma+j})$ terms, with $j = 1$, 2, and 3, vanish. For the $O(k^\gamma)$ term, we find the coefficient $-\pi B\lambda\gamma(\gamma-2)(\gamma-3)/\sin\pi\gamma$, which must match the coefficient $B$ on the left-hand side, yielding Eq. (46). We neglect all the terms of lower order in $k$. This includes the linear terms, due to the assumption $\gamma > 1$.

## APPENDIX D: ESTIMATES FOR THE NETWORK-COUPLING SCALING BOUNDS

In this Appendix, we derive the estimates used to establish the scaling bounds in Sec. V. First, we derive the estimate in Eq. (49). A single iteration of Eq. (13) produces the equation

$$\begin{aligned} m_k = \psi\Big(1+\lambda\int_0^N K(k,n)dn \\ +\lambda^2\int_0^N\int_0^N K(k,n)K(n,p)m_p\,dn\,dp\Big). \end{aligned} \tag{D1}$$

Noting that all the terms on the right-hand side of this inequality are non-negative, we see that $m_k$ exceeds the sum of the first two terms alone. The second term is easily calculated to equal $\psi\lambda k$ using Eqs. (14) and (1), and so the estimate (49) follows.

Second, we show how the estimate in Eq. (51) follows from the weak-correlation condition (50). In particular, when this condition is satisfied, Eq. (14) implies that the kernel $K(k,n)$ in Eq. (13) satisfies the estimate $K(k,n) \leqslant \eta k n P_{\rm in}(n)/\mu$, which further implies that the $i$th iterated kernel, $K_i(k,n)$ in Eq. (16c), satisfies the estimate

$$\begin{aligned} K_i(k,n) &\leqslant \int_0^N\cdots\int_0^N \frac{\eta k y_1 P_{\rm in}(y_1)}{\mu}\,\frac{\eta y_1 y_2 P_{\rm in}(y_2)}{\mu}\cdots \\ &\quad\times\frac{\eta y_{i-1} n P_{\rm in}(n)}{\mu}dy_1\ldots dy_{i-1} \\ &= \eta k\left(\frac{\eta\langle n^2\rangle_N}{\mu}\right)^{i-1}\frac{n P_{\rm in}(n)}{\mu}. \end{aligned} \tag{D2}$$

Using Eq. (16a), we thus conclude that the $i$th coefficient $\phi_i(k)$ in the Liouville-Neumann series (15) can be bounded by $\phi_i(k) \leqslant \psi\eta k(\eta\langle n^2\rangle_N/\mu)^{i-1}$. Summing the geometric-series majorant obtained from this estimate now implies that the entire Louiville-Neumann series for the pulse rate $m_k$ can be bounded by the estimate in Eq. (51).

To derive the estimate in Eq. (56) from the statistical symmetry of the network, we iterate Eq. (13) twice, and integrate the resulting equation over $k$ with the wieght $P_{\rm in}(k)$. We thus obtain the following equation for the pulse rate $m_k$ averaged over the entire network:

$$\begin{aligned} \bar m = \int_0^N P_{\rm in}(k)m_k dk &= \psi + \psi\lambda\mu \\ &+\psi\lambda^2\int_0^N\int_0^N\int_0^N P_{\rm in}(k)K(k,y_1)K(y_1,y_2)dy_1dy_2dk \\ &+\lambda^3\int_0^N\int_0^N\int_0^N\int_0^N P_{\rm in}(k) \\ &\times K(k,y_1)K(y_1,y_2)K(y_2,y_3)m_{y_3}dy_3dy_2dy_1dk. \end{aligned} \tag{D3}$$

Using Eq. (14), we can rewrite the triple integral multiplying $\psi\lambda^2$ in this equation as

$$\begin{aligned} \mu^2\int_0^N\int_0^N\int_0^N \frac{T(y_1,k)T(y_2,y_1)}{P_{\rm in}(y_1)}dy_1dy_2dk \\ = \mu\int_0^N\int_0^N y_1T(y_2,y_1)dy_2dy_1 \\ = \int_0^N y_1^2P_{\rm in}(y_1)dy_1 = \langle n^2\rangle_N, \end{aligned} \tag{D4}$$

where we have used Eqs. (55) and (1) to arrive at the expressions on the second and third lines, respectively. Recall that Eq. (55) follows from the assumed statistical symmetry of the network. Equation (D4) implies that Eq. (D3) can be rewritten as Eq. (56).


[1] O. Omidvar and J. Dayhoff, eds., *Neural Networks and Pattern Recognition* (Academic Press, San Diego, Chestnut Hill, London, 1997).

[2] J. Johnson, M. Padgett, and O. Omidvar, IEEE Trans. Neural Networks **10**, 461 (1999).

[3] S. Strogatz, Nature (London) **410**, 268 (2001).

[4] W. Gerstner and W. Kistler, *Spiking Neuron Models—Single Neurons, Populations, Plasticity* (Cambridge University Press, New York, 2002).

[5] A. N. Burkitt, Biol. Cybern. **95**, 1 (2006).

[6] A. N. Burkitt, Biol. Cybern. **95**, 97 (2006).

[7] A. Barrat, M. Barthélemy, and A. Vespignani, *Dynamical Processes on Complex Networks* (Cambridge University Press, Cambridge, New York, 2008).

[8] T. Lindblad and J. M. Kinser, *Image Processing Using Pulse-Coupled Neural Networks* (Springer, Berlin, Heidelberg, 2010).

[9] Y. Ma, K. Zhan, and Z. Wang, *Applications of Pulse-Coupled Neural Networks* (Springer, New York, 2010).

[10] A. Barabasi and R. Albert, Science **286**, 509 (1999).

[11] S. N. Dorogovtsev and J. F. F. Mendes, Adv. Phys. **51**, 1079 (2002).

[12] M. Newman, SIAM Rev. **45**, 167 (2003).
[13] S. Boccaletti, V. Latora, Y. Moreno, M. Chavez, and D.-U. Hwang, Phys. Rep. **424**, 175 (2006).
[14] D. C. Somers, S. B. Nelson, and M. Sur, J. Neurosci. **15**, 5448 (1995).
[15] T. W. Troyer, A. E. Krukowski, N. J. Priebe, and K. D. Miller, J. Neurosci. **18**, 5908 (1998).
[16] D. McLaughlin, R. Shapley, M. Shelley, and J. Wielaard, Proc. Natl. Acad. Sci. USA **97**, 8087 (2000).
[17] D. J. Wielaard, M. Shelley, D. McLaughlin, and R. Shapley, J. Neurosci. **21**, 5203 (2001).
[18] D. Cai, A. Rangan, and D. McLaughlin, Proc. Natl. Acad. Sci. USA **102**, 5868 (2005).
[19] A. V. Rangan, D. Cai, and D. W. McLaughlin, Proc. Natl. Acad. Sci. USA **102**, 18793 (2005).
[20] D. Fitzpatrick, J. S. Lund, and G. G. Blasdel, J. Neurosci. **5**, 3329 (1985).
[21] J. Lund, J. Comp. Neurol. **257**, 60 (1987).
[22] E. Callaway and A. Wiser, Visual Neurosci. **13**, 907 (1996).
[23] E. Callaway, Annu. Rev. Neurosci. **21**, 47 (1998).
[24] W. H. Bosking, Y. Zhang, B. Schofield, and D. Fitzpatrick, J. Neurosci. **17**, 2112 (1997).
[25] L. C. Sincich and G. G. Blasdel, J. Neurosci. **21**, 4416 (2001).
[26] A. Angelucci, J. B. Levitt, E. J. S. Walton, J.-M. Hupé, J. Bullier, and J. S. Lund, J. Neurosci. **22**, 8633 (2002).
[27] A. Angelucci and J. Bullier, J. Phys. (Paris) **97**, 141 (2003).
[28] J. Lund, A. Angelucci, and P. Bressloff, Cereb. Cortex **12**, 15 (2003).
[29] N. Ramnani, T. E. J. Behrens, W. Penny, and P. M. Matthews, Biol. Psychiatry **56**, 613 (2004).
[30] A. A. Ioannides, Curr. Opin. Neurobiol **17**, 161 (2007).
[31] J. C. Reijneveld, S. C. Ponten, H. W. Berendse, and C. J. Stam, Clin. Neurophysiol. **118**, 2317 (2007).
[32] C. J. Stam and J. C. Reijneveld, Nonlinear Biomed. Phys. **1**, 3 (2007).
[33] M. P. van den Heuvel, C. J. Stam, M. Boersma, and H. E. Hulshoff Pol, Neuroimage **43**, 528 (2008).
[34] M. Guye, F. Bartolomei, and J.-P. Ranjeva, Curr. Opin. Neurol. **21**, 393 (2008).
[35] D. A. Fair, A. L. Cohen, J. D. Power, N. U. F. Dosenbach, J. A. Church, F. M. Miezin, B. L. Schlaggar, and S. E. Petersen, PLoS Comput. Biol. **5**, e1000381 (2009).
[36] C. J. Stam, Int. J. Psychophysiol. **77**, 186 (2010).
[37] D. Cai, L. Tao, M. Shelley, and D. McLaughlin, Proc. Natl. Acad. Sci. USA **101**, 7757 (2004).
[38] D. Cai, L. Tao, A. V. Rangan, and D. W. McLaughlin, Commun. Math. Sci. **4**, 97 (2006).
[39] A. Treves, Network **4**, 259 (1993).
[40] M. Shelley and D. McLaughlin, J. Comp. Neurosci. **12**, 97 (2002).
[41] K. Klemm and V. M. Eguíluz, Phys. Rev. E **65**, 057102 (2002).
[42] P. L. Krapivsky and S. Redner, Phys. Rev. E **63**, 066123 (2001).
[43] M. S. Shkarayev, G. Kovačič, A. V. Rangan, and D. Cai, Europhys. Lett. **88**, 50001 (2009).
[44] V. M. Eguíluz, D. R. Chialvo, G. A. Cecchi, M. Baliki, and A. V. Apkarian, Phys. Rev. Lett. **94**, 018102 (2005).
[45] M. Kaiser, R. Martin, P. Andras, and M. Young, Eur. J. Neurosci. **25**, 3185 (2007).
[46] P. Bonifazi, M. Goldin, M. A. Picardo, I. Jorquera, A. Cattani, G. Bianconi, A. Represa, Y. Ben-Ari, and R. Cossart, Science **326**, 1419 (2009).
[47] E. Bullmore and O. Sporns, Nat. Rev. Neurosci. **10**, 186 (2009).
[48] M. E. J. Newman, Phys. Rev. Lett. **89**, 208701 (2002).
[49] M. Shelley and L. Tao, J. Comput. Neurosci. **11**, 111 (2001).
[50] R. Courant and D. Hilbert, *Methods of Mathematical Physics*, Vol. 1 (Wiley, New York, 1989).
[51] G. Kovačič, L. Tao, A. V. Rangan, and D. Cai, Phys. Rev. E **80**, 021904 (2009).
[52] E. N. Gilbert, Ann. Math. Stat. **30**, 1141 (1959).
[53] P. Erdös and A. Rényi, Publ. Math. **6**, 290 (1959).
[54] P. Erdös and A. Rényi, Publ. Math. Inst. Hungarian Acad. Sci. **5**, 17 (1960).
[55] M. Catanzaro, M. Boguna, and R. Pastor-Satorras, Phys. Rev. E **71**, 027103 (2005).
[56] D. Schmidt, J. Best, and M. S. Blumberg, Random Graph and Stochastic Process Contributions to Network Dynamics, Discrete and Continuous Dynamical Systems, Supplement 2011, pp. 1279–1288.
[57] T. Ohira and R. Sawatari, Phys. Rev. E **58**, 193 (1998).
[58] A. Broder, R. Kumar, F. Maghoul, P. Raghavan, S. Rajagopalan, R. Stata, A. Tomkins, and J. Wiener, Comput. Networks **33**, 309 (2000).
[59] S. Jespersen, I. M. Sokolov, and A. Blumen, Phys. Rev. E **62**, 4405 (2000).
[60] S. A. Pandit and R. E. Amritkar, Phys. Rev. E **63**, 041104 (2001).
[61] A. Arenas, A. Díaz-Guilera, and R. Guimerà, Phys. Rev. Lett. **86**, 3196 (2001).
[62] L. A. Adamic, R. M. Lukose, A. R. Puniyani, and B. A. Huberman, Phys. Rev. E **64**, 046135 (2001).
[63] J. Lahtinen, J. Kertész, and K. Kaski, Phys. Rev. E **64**, 057105 (2001).
[64] K.-I. Goh, B. Kahng, and D. Kim, Phys. Rev. Lett. **87**, 278701 (2001).
[65] R. Sole and S. Valverde, Physica A **289**, 595 (2001).
[66] B. J. Kim, C. N. Yoon, S. K. Han, and H. Jeong, Phys. Rev. E **65**, 027103 (2002).
[67] E. Almaas, R. V. Kulkarni, and D. Stroud, Phys. Rev. Lett. **88**, 098101 (2002).
[68] R. Guimerà, A. Díaz-Guilera, F. Vega-Redondo, A. Cabrales, and A. Arenas, Phys. Rev. Lett. **89**, 248701 (2002).
[69] F. Menczer, Proc. Natl. Acad. Sci. USA **99**, 14014 (2002).
[70] D. R. White and M. Houseman, Complexity **8**, 72 (2002).
[71] J. Lahtinen, J. Kertész, and K. Kaski, Physica A **311**, 571 (2002).
[72] P. Holme, Adv. Complex Syst. **6**, 163 (2003).
[73] A. P. S. de Moura, A. E. Motter, and C. Grebogi, Phys. Rev. E **68**, 036106 (2003).
[74] E. Almaas, R. V. Kulkarni, and D. Stroud, Phys. Rev. E **68**, 056105 (2003).
[75] J. D. Noh and H. Rieger, Phys. Rev. Lett. **92**, 118701 (2004).
[76] J. D. Noh and H. Rieger, Phys. Rev. E **69**, 036111 (2004).
[77] B. Tadić, S. Thurner, and G. J. Rodgers, Phys. Rev. E **69**, 036102 (2004).
[78] N. Masuda and N. Konno, Phys. Rev. E **69**, 066113 (2004).
[79] H. Zhu and Z.-X. Huang, Phys. Rev. E **70**, 036117 (2004).
[80] A. P. S. de Moura, Phys. Rev. E **71**, 066114 (2005).

[81] R. Germano and A. P. S. de Moura, Phys. Rev. E **74**, 036117 (2006).
[82] H. Lin and C.-X. Wu, Eur. Phys. J. B **51**, 543 (2006).
[83] D. Helbing, D. Armbruster, A. S. Mikhailov, and E. Lefeber, Physica A **363**, xi (2006).
[84] K. A. Newhall, G. Kovačič, P. R. Kramer, D. Zhou, A. V. Rangan, and D. Cai, Commun. Math. Sci. **8**, 541 (2010).
[85] K. A. Newhall, G. Kovačič, P. R. Kramer, and D. Cai, Phys. Rev. E **82**, 041903 (2010).
[86] K. A. Newhall, M. S. Shkarayev, P. R. Kramer, G. Kovačič, and D. Cai, Synchrony in Stochastically Driven Neuronal Networks with Complex Topologies, preprint (2012).
[87] H. R. Wilson and J. D. Cowan, Biophys. J. **12**, 1 (1972).
[88] H. Wilson and J. Cowan, Kybernetik **13**, 55 (1973).
[89] R. Ben-Yishai, R. Bar-Or, and H. Sompolinsky, Proc. Natl. Acad. Sci. USA **92**, 3844 (1995).
[90] P. Bressloff, J. Cowan, M. Golubitsky, P. Thomas, and M. Wiener, Philos. Trans. R. Soc. London B **356**, 299 (2001).
[91] B. Knight, J. Gen. Physiol. **59**, 734 (1972).
[92] W. Wilbur and J. Rinzel, J. Theor. Biol. **105**, 345 (1983).
[93] L. F. Abbott and C. van Vreeswijk, Phys. Rev. E **48**, 1483 (1993).
[94] T. Chawanya, A. Aoyagi, T. Nishikawa, K. Okuda, and Y. Kuramoto, Biol. Cybern. **68**, 483 (1993).
[95] D. J. Amit and N. Brunel, Cereb. Cortex **7**, 237 (1997).
[96] G. Barna, T. Grobler, and P. Erdi, Biol. Cybern. **79**, 309 (1998).
[97] J. Pham, K. Pakdaman, J. Champagnat, and J. Vibert, Neural Networks **11**, 415 (1998).
[98] N. Brunel and V. Hakim, Neural. Comput. **11**, 1621 (1999).
[99] W. Gerstner, Neural Comput. **12**, 43 (2000).
[100] A. Omurtag, B. Knight, and L. Sirovich, J. Comp. Neurosci. **8**, 51 (2000).
[101] A. Omurtag, E. Kaplan, B. Knight, and L. Sirovich, Network **11**, 247 (2000).
[102] D. Nykamp and D. Tranchina, J. Comput. Neurosci. **8**, 19 (2000).
[103] D. Nykamp and D. Tranchina, Neural Comput. **13**, 511 (2001).
[104] E. Haskell, D. Q. Nykamp, and D. Tranchina, Network: Comput. Neural Syst. **12**, 141 (2001).
[105] A. Casti, A. Omurtag, A. Sornborger, E. Kaplan, B. Knight, J. Victor, and L. Sirovich, Neural Comput. **14**, 957 (2002).
[106] N. Fourcaud and N. Brunel, Neural Comput. **14**, 2057 (2002).
[107] A. V. Rangan and D. Cai, Phys. Rev. Lett. **96**, 178101 (2006).
[108] E. Cinlar, in *Stochastic Point Processes: Statistical Analysis, Theory, and Applications*, edited by P. Lewis (Wiley, New York, 1972), pp. 549–606.
[109] R. Courant and D. Hilbert, *Methods of Mathematical Physics*, Vol. 2 (Wiley, New York, 1989).
[110] F. John, *Partial Differential Equations*, Applied Mathematical Sciences, Vol. 1 (Springer-Verlag, New York, Heidelberg, Berlin, 1981).
[111] W. Feller, *An Introduction to Probability Theory and Its Applications* (Wiley, New York, 1968).